Insights into Water Mass Circulation and Origins in the Central Arctic Ocean from in-situ Dissolved Organic Matter Fluorescence.

Colin A Stedmon[1], Rainer M. W. Amon[2], Dorothea Bauch[3], Astrid Bracher[4], Rafael Gonçalves-Araujo[1], Mario Hoppmann[5], Richard A. Krishfield[6], Samuel Laney[6], Benjamin Rabe[7], Heather E Reader[8], and Mats Anders Granskog[9]

[1]Technical University of Denmark
[2]Texas A&M University at Galveston
[3]GEOMAR Helmholtz Centre for Ocean Research Kiel
[4]Alfred Wegener Institute
[5]AWI, Germany
[6]Woods Hole Oceanographic Institution
[7]Alfred-Wegener-Institut Helmholtz-Zentrum für Polar- und Meeresforschung
[8]Memorial University of Newfoundland
[9]Norwegian Polar Institute

November 30, 2022

Abstract

The Arctic Ocean receives a large loading of dissolved organic matter (DOM) from its catchment and shelf sediments, which can be traced across much of the basin. This signature can be used as a tracer of water mass circulation. On the shelf seas, the combination of freshwater loading from rivers and ice formation modify water mass densities and mixing considerably. These waters are the source of the halocline layer that covers much of the Arctic ocean. Our knowledge of the origins, formation and maintenance of the halocline has mostly arisen from CTD profiles and chemical tracers such as oxygen stable isotopes and inorganic nutrients, but the halocline also contains elevated levels of DOM (DOM). Here we demonstrate how this can be used as a tracer and help improve our understanding of ocean circulation. DOM fluoresce can be measured using in-situ fluorometers and mounted on autonomous platforms these can provide high spatial resolution measurements. Here we present data derived from several Ice Tethered Profilers. The data offer a unique spatial coverage of the distribution of DOM in the surface 800m below Arctic ice. Water mass analysis using temperature, salinity and DOM fluorescence, clearly distinguishs the halocline contribution of Siberian terrestrial DOM and marine DOM from the Chuckchi shelf. The findings offer a new approach to trace the distribution of Pacific waters and its export from the Arctic Ocean. Our results indicate the potential to extend the approach to fraction freshwater contributions from, sea ice melt, riverine discharge and Pacific water.

Insights into Water Mass Circulation and Origins in the Central Arctic Ocean from in-situ Dissolved Organic Matter Fluorescence.

Colin A. Stedmon[1*]; Rainer M.W. Amon[2,3], Dorothea Bauch[4,5] Astrid Bracher[6,7,] Rafael Gonçalves−Araujo[1]; Mario Hoppmann[6]; Richard Krishfield[8]; Samuel Laney[8]; Ben Rabe[6]; Heather Reader[9]; Mats A. Granskog[10]

[1] National Institute for Aquatic Resources, Technical University of Denmark, Lyngby, Denmark.

[2] Texas A&M University, Department of Marine and Coastal Environmental Science, Galveston, USA

[3] Texas A&M University, Department of Oceanography, College Station, USA

[4] Leibniz Laboratory, University of Kiel, Kiel, Germany

[5] GEOMAR Helmholtz Centre for Ocean Research Kiel, Kiel, Germany

[6] Alfred-Wegener-Institut Helmholtz-Zentrum für Polar- und Meeresforschung, Bremerhaven, Germany

[7] Institute of Environmental Physics, Faculty of Physics and Electrical Engineering, University Bremen, Bremen, Germany

[8] Woods Hole Oceanographic Institution, Woods Hole, Massachusetts, USA.

[9] Department of Chemistry, Memorial University of Newfoundland, St John's, Canada.

[10] Norwegian Polar Institute, Fram Centre, Tromsø, Norway.

Corresponding author: Colin A. Stedmon (cost@aqua.dtu.dk)

Key Points:

- Dissolved organic matter fluorescence can distinguish different Arctic water mass origins
- Siberian and Chuckchi shelf waters can be separated based on their fluorescence to salinity relationship
- There is also a potential to fractionate freshwater contrituion from seaice, Pacific water and river water.
- Fluorescence can be traced by in sity profilers and offer a valuable addition to autonomous profilers

Abstract

The Arctic Ocean receives a large loading of dissolved organic matter (DOM) from its catchment and shelf sediments, which can be traced across much of the basin. This signature can be used as a tracer of water mass circulation. On the shelf seas, the combination of freshwater loading from rivers and ice formation modify water mass densities and mixing considerably. These waters are the source of the halocline layer that covers much of the Arctic ocean. Our knowledge of the origins, formation and maintenance of the halocline has mostly arisen from CTD profiles and measurements of chemical tracers such as oxygen stable isotopes and inorganic nutrients, but the halocline also contains elevated levels of colored DOM (CDOM). Here we demonstrate how this can be used as a tracer and help improve our understanding of ocean circulation in the Arctic. A fraction of the organic compounds present in DOM fluoresce and this can be measured using in-situ fluorometers mounted on CTDs. Deployed on autonomous platforms these can provide high spatial resolution measurements. Here we present the results of an analysis of data derived from several Ice Tethered Profilers. The data offer a unique spatial coverage of the distribution of DOM in the surface 800m below Arctic ice. Water mass analysis using temperature, salinity and DOM fluorescence, can clearly distinguish between the contribution of Siberian terrestrial DOM and marine DOM from the Chuckchi shelf to the waters of the halocline. The findings offer a new approach to trace the distribution of Pacific waters and its export from the Arctic Ocean. Our results indicate the potential to extend the approach to fraction freshwater contributions from, sea ice melt, riverine discharge and Pacific water.

1 Introduction

The Arctic Ocean is surrounded by expansive shelf seas which influence ocean circulation and seawater properties (Figure 1). Shallow depths restrict deep water exchange to only occur in the Fram Strait. Much of the surface water inflow occurs over the expansive shelf sea areas, where river runoff and extensive seasonal sea ice formation and melt modify the physical and chemical properties. Inflowing waters from the Pacific and Atlantic also loose heat to the atmosphere and are cooled during their passage over the shelves (Dmitrenko et al., 2009; Rudels et al., 1996; Rudels et al., 2000; Shimada, 2005). These waters are gradually modified and diluted by the freshwater discharge from major rivers with catchments in North America and Siberia (Haine et al., 2015; Overeem & Syvitski, 2010; Peterson et al., 2002; Serreze et al., 2006). Sea ice formation and subsequent export of ice off the shelf partially counteracts this dilution (Bauch et al., 2009, 2011). Brine rejection results in the formation of shelf waters very close to freezing temperature and with slightly increased salinity (as well as other dissolved constituents).

The chemical composition of inflowing oceanic water is also altered during its passage over the shelves. Rivers supply high concentrations of terrestrial dissolved organic matter (DOM) (Amon et al., 2012). While inorganic nutrient concentrations in Arctic rivers are comparable to oceanic concentrations (Holmes et al., 2012), dissolved organic carbon (DOC) concentrations are an order of magnitude higher than in inflowing ocean water (Anderson & Amon, 2015). Further, interactions with shelf sea sediments also influence the chemical composition of these waters, as degradation and dissolution of particulate organic matter results in high porewater concentrations of DOC which subsequently diffuse to overlying waters (Chen

et al., 2016). Concentrations of nutrients in shelf bottom waters are also higher as a result of elevated rates of organic matter mineralization (Bauch et al., 2011; Dmitrenko et al., 2011; Jones & Anderson, 1986). Denitrification in organic rich sediments is a sink for nitrate and results in shelf waters having a nitrogen deficit relative to phosphate, in comparison to sub-Arctic ocean waters (Anderson et al., 2013; Codispoti et al., 2005; Hardison et al., 2017; Jones & Anderson, 1986). Passage over the shelf therefore imparts a detectable chemical signature which is then entrained into the larger scale circulation of the Arctic basin.

Surface waters of the Arctic Ocean are often referred to as the Polar Mixed Layer (PML; e.g. Korhonen et al., 2013), which is shaped by repeated convective mixing due to brine release from seasonal ice formation. It is often re-stratified during the melting season, bounded at the bottom by a temperature minimum that is a remnant of the deeper mixed layer from the previous winter's convection (Korhonen et al., 2013; Peralta-Ferriz & Woodgate, 2015; Rudels et al., 2004). A striking characteristic of the water column in the Arctic Ocean is the widespread presence of a halocline layer (HL) (Coachman & Aagaard, 1974), which consists of cold waters with temperatures close to freezing point for their given salinity, and salinities ranging between 28-34.8 (Korhonen et al., 2013). The HL is fed by brine rejection (associated with sea ice formation) and convection occurring in open waters (Steele & Boyd, 1998) or in shelf seas and subsequently advected off-shore (Aagaard et al., 1981). Halocline waters can extend from near the surface (in areas of formation) to as deep as ~300 m in the Canada Basin. The HL separates surface waters from warmer waters of Atlantic origin below (hereafter referred to as Atlantic Water). The stratification maintained by the halocline facilitates the formation and persistence of sea ice in the Arctic as the PML is largely insulated from contact with warmer Atlantic waters below (Aagaard et al., 1981; Toole et al., 2010). Ice free waters of the greater Arctic region, are as such due to the absence of a persistent cold halocline layer (Polyakov et al., 2020) or increased retention of summer heat in PML (Timmermans et al., 2018).

The HL in the Arctic Ocean differs in composition and structure depending on location. The lower halocline (LHC) has its origins in waters from the Atlantic and extends from a salinity of 34 to the depth of the 0 C isotherm (Korhonen et al., 2013). It is formed near the inflow regions of Atlantic Water (AW) north of the Fram Strait, the southern Nansen Basin and the Barents Sea (B. Rudels et al., 1996). This forms the main transition between the PML, which has properties that vary seasonally, and the deeper AW with potential temperatures above 0 ºC. In the Canada Basin the HL extends deeper and is composed by two distinct layers: the upper halocline (UHC), right underneath the PML (temperature minimum) and the LHC originating from the Eurasian Basin (Rudels et al., 2004). The UHC is composed of low salinity water from the Pacific inflow (S~32.5) (Coachman & Barnes, 1961). This is subject to seasonal variability and lateral intrusion of Pacific or dense water formed during ice formation on the shelves (D. Bauch et al., 2014; Jones & Anderson, 1986). Contributions to the UHC are Pacific Summer Water (PSW) recognizable as a distinct temperature maximum (> -1 C) with salinities between 31 and 33 (Steele et al., 2004) and below this is a temperature minimum representing Pacific Winter Water (PWW) with salinities of about 33.1 (Coachman & Barnes, 1961). Above the UHC in the Canada Basin, near surface temperature maximum (NSTM) can develop due to summertime warming from solar radiation which is subsequently covered by a thin surface layer of fresh water from ice melt (Jackson et al., 2010).

Another distinct oceanographic feature in the central Arctic is the Transpolar Drift (TPD). This is an ice and surface ocean current that connects the East Siberian and Laptev seas

to the Fram Strait (Morison et al., 2012; Steele et al., 2004) and segregates the surface water of the Arctic Ocean. The positioning of the TPD can vary between generally along the Lomonosov Ridge in periods with low Arctic Oscillation (AO) index to extending more towards the Chuckchi shelf in periods with a high AO (Figure 1)(Morison et al., 2012). As such the relative contributions of waters from the Siberian shelf (Atlantic origin) and Chuckchi shelf (Pacific) can vary. The TPD carries a clear terrigenous signal from the Siberian shelves across the Arctic and onwards to the North Atlantic (Charette et al., 2020; Williford et al., 2021), but can also entrain a Pacific water signal, most noticeable as a lack of nitrate and excess silicate (Anderson et al., 2013; Dorothea Bauch et al., 2011; Jones & Anderson, 1986; McLaughlin et al., 2004), or by having distinctly different DOM properties (Amon et al , 2003; Gonçalves-Araujo et al., 2016; Stedmon et al., 2011; Williford et al., 2021). These geochemical signals can therefore be used as a tracers of water origin and circulation in the Arctic Ocean.

Much of the empirical knowledge and insight on the origins and characteristics of the Arctic halocline has been based on temperature and salinity profiles, and supplemented with water chemistry measurements, primarily inorganic nutrients. The increasingly widespread deployment of additional biogeochemical sensors on profiling instruments offers higher resolution measurements and an opportunity to further resolve processes involved with HL formation, and source fractionation of freshwater distribution (Athanase et al., 2019; Bertosio et al., 2020; Boles et al., 2020; Dmitrenko et al., 2019; Laney et al., 2014). A fraction of the organic compounds present in DOM fluoresce and this can be used as a proxy for dissolved organic carbon in the Arctic (Amon et al, 2003; Gonçalves-Araujo et al., 2016). It provides a rapid and sensitive method for characterizing and tracing DOM (Stedmon & Nelson, 2015). The major advantage of the approach is that it can be measured in situ with readily available single- or multichannel fluorometers (Belzile et al., 2006; Makarewicz et al., 2018). This potentially offers high spatial resolution measurements although the full potential has not been realized due to the lack of a robust and agreed upon cross-sensor calibration procedure. Initial studies from specific instruments have demonstrated its utility for the study of DOM biogeochemistry and water mass tracing in the Arctic Ocean (Amon et al., 2003; Cooper et al., 2005; Dmitrenko et al., 2019; Williford et al., 2021).

Here we present a comprehensive intercalibration and analysis of legacy data derived from Ice Tethered Profilers (ITPs) deployed in the central Arctic Ocean which have been equipped with single-channel organic matter fluorometers. Building on the earlier data obtained from the Canada Basin (Laney et al., 2014) and expanding the analysis to deeper waters, the data offers unique temporal and spatial coverage of the distribution of DOM in the 800m below Arctic sea ice. We demonstrate the utility of high resolution in situ DOM fluorescence as a tracer of Arctic circulation. Water mass analysis using temperature, salinity and DOM fluorescence provides new insight into the close connectivity between the halocline layer composition and linkage to sea-ice formation in shelf waters influenced by river run off. This infers that winter sea-ice formation on the shelf plays an important role in maintaining stratification in the surface 500 m of much of the Arctic Ocean, which is in turn a major factor controlling sea ice extent in the central Arctic. Our results also suggest that DOM in the central Arctic Ocean mixes largely conservatively once it has entered the deep and ice-covered central basin and can therefore be used as a tracer of waters of shelf origin and to detect surface freshening due to sea ice melt with in situ observations.

2 Materials and Methods

The data used for the analysis is summarized in Table 1. It mainly consists of measurements made as part of the Woods Hole Oceanographic Institution ITP program (Krishfield et al., 2008; Toole et al., 2011) (http://www.whoi.edu/itp) and the FRontiers in Arctic marine Monitoring (FRAM) observatory (https://www.awi.de/en/expedition/observatories/ocean-fram.html). These observations are complemented with data from ship-based profiles from two research cruises: Arctic GEOTRACES GN04 program cruise (PS94, TRANSARC II) with R/V Polarstern and a cruise on the East Greenland Shelf with R/V Dana in 2012 as part of the Danish NAACOS project.

The ITP data are level 3 data products pressure-bin-averaged at 1-db vertical resolution. The ship-based observations are 1 m bin averages. Only data for the surface 800m are included in this analysis as this represented the depths covered by the ITP data. Figure 1 shows the spatial coverage of the different sensor platforms. In conjunction with the two oceanographic cruises, water samples were collected and used to calibrate the CDOM sensors mounted on the ships CTD. ITP93 was deployed during the PS94 cruise and there is an overlap between the first ITP profiles and a station located at the deployment site. Data from the NAACOS cruise is used to independently verify the applied intercalibration procedure. The profiles from both cruises are included in the data analysis. The instrument package design for ITP48-65 and a presentation of the result for the surface 100m has been published earlier (Laney et al., 2014).

Water samples collected for CDOM analysis from the two cruises were filtered through a 0.2 μm capsule Millipore filter (part # KVGLA04HH3) attached directly to the rosette sampler bottles once on deck. Then absorption and fluorescence properties of DOM were measured shortly afterwards onboard. CDOM fluorescence was measured on a Horiba Aqualog spectrofluorometer and CDOM absorption was measured on either a Perkin Elmer Lambda 35 (PS94) or a Shimadzu UVPC2501 (NAACOS) using a 10cm quartz cuvette and fresh derived pure water (MilliQ with UV lamp) as a blank. Fluorescence data were processed according to the guidelines in (Murphy et al., 2010) resulting in inner filter corrected spectra and fluorescence intensities in Raman Units, nm^{-1} (Lawaetz & Stedmon, 2009). The fluorescence intensities at excitation 350 and emission 450 nm were used to calibrate the voltage signal from the CTD mounted fluorometers. It should be noted that the DrHaardt instrument has a slightly different wavelength range (excitation 350-460nm, emission 550nm) but that the signal was linearly correlated to the excitation 350 nm and emission 450 nm signal (Figure S1). Fluorescence at these wavelengths (ultraviolet excitation and visible emission) is often referred to a “humic” due to the similar character to soil extracted organic matter, however it represents a persistent ubiquitous fluorescent signal found in natural waters which originates either from terrestrial organic matter supplied by rivers or from the degradation of marine organic matter (Stedmon & Cory, 2014).

ITP CDOM Sensor Intercalibration

The organic matter fluorescence signal from each ITP was first smoothed using a moving average algorithm with a window of 20 m, in order to better recover DOM fluorescence information at the low concentrations characteristic of the central Arctic Ocean. Thereafter the data were checked for fluorescence sensor drift or baseline shifts by plotting the average and standard deviations for each profile for measurements from depths greater than 700m for temperature (q), practical salinity (S) and DOM fluorescence. At these depths the fluorescence signal was very stable and sensor drift and baseline shifts could be easily identified as either a systematic gradually changing fluorescence signal (typically over first month of a deployment, despite little geographic movement) or a sudden shift (from one day to the next) in the deep-water averages, whilst q and S properties otherwise remained constant. It is likely that these were caused by either gradual biofouling or episodic attachment of matter onto the fluorometer sensor lens. These were corrected for by either subtracting a polynomial fit of the sensor drift or by subtracting a constant value from the remaining data after a given date.

Initial comparison of the baseline corrected ITP data indicated that the fluorescence sensors from each platform required intercalibration (Figure S2). Although the data from the majority of the sensors appear to be either factory or laboratory calibrated pre-deployment to a fluorescence standard (quinine sulfate) there were still notable differences manifesting mostly as different offsets (varying in raw FL units from -10 to +3). The post deployment intercalibration was carried out in two stages. The first step was to calibrate the CTD mounted fluorometer from PS94 to the water samples collected and measured onboard. A linear calibration curve was obtained converting the voltage output signal to fluorescence in Raman Units, [nm^{-1}] (Figure S1).

Secondly θ-S plots of individual station profiles in the whole dataset were examined for a common region in θ-S space, representing the same waters were sampled by all platforms and ignoring surface measurements. The region of mixing of lower halocline waters and AW, with salinities ranging from 34.2 to 34.8, was identified to have the best overlap, but the data had to be segregated with respect to the Eurasian and Canada Basins as there were notable differences in q-S between the two. For the Eurasian profiles the lower salinity data were colder and the (high salinity) temperature maximum was warmer (Figure S3) as explained in Rudels et al., (2004). ITP48 sampled both water types during its deployment and could therefore be used to intercalibrate the data between basins.

Data from selected profiles for each sensor were used for the intercalibration to the PS94 CTD mounted calibrated fluorescence (Figure S3). A linear regression between salinity (34.2 to 34.8) and DOM fluorescence was performed for each sensor and used to convert the measured fluorescence to calibrated fluorescence in Raman Units. In order to assess the success of this procedure, two comparisons were made. First, ITP93 was deployed during the PS94 cruise and there was an overlap station from the shipboard CTD on 21 Sep 2015 and the first profile of the ITP on 24 Sep 2015 (Figure S4). Second, the intercalibration approach could be assessed using data from a separate cruise (NAACOS, 2012), calibrated with its own measurements onboard. This was done in DOM-S space. Although modifications to polar waters and return AW do occur as it is transported along the Greenland shelf, the clear overlap in the property-property plots offered confidence to the success of the intercalibration of the sensors (Figure S4).

3 Results

The compiled dataset offers good coverage of contrasting regions of the Arctic Ocean, namely the Eurasian Basin (Nansen Basin, Gakkel Ridge and Amundsen Basin), the Transpolar Drift (Lomonosov Ridge) and Canada Basin (Makarov Basin, Alpha Ridge and Beaufort Sea) (Figure 1). Histograms of the θ-S and DOM-S properties of the dataset indicate that the majority of the volume of the upper 800m in the central Arctic basins has salinities between 32 and 34.8 and have potential temperatures ranging from close to their freezing point and increasing to just under 2 °C (Figure 2). The data at lower salinities (<32) stem from the surface 50 m but diverge at salinity of about 30.5, with Eurasian Basin waters for the most part having temperatures very close to freezing and Beaufort Sea surface waters being responsible for the warmer temperatures (Figure 2).

At S < 34 there is considerable spread in DOM fluorescence, revealing two major branches of data (Figure 2), with the remaining data falling between (while the temperature shows little spread here). The upper branch (higher fluorescence) is an approximately linear extension of the inverse relationship between DOM fluorescence and salinity seen at salinities greater than 34. The lower branch has a local DOM maximum at salinities between 32 and 33, then decreases with decreasing salinity. The upper branch originates from surface waters in the Eurasian Basin which are influenced by the TPD while the lower branch represents subsurface waters in the Beaufort Sea originating from the Chukchi Sea.

These patterns are evident in three representative sections shown in Figure 3. The surface waters (upper 50m) of the Beaufort Sea (ITP64) are characterized by low salinity and low DOM fluorescence waters with variable temperature (local temperature maxima and minima). Directly below the ice, temperatures are low but increase to a subsurface maximum between 50 and 100 m. Below this there is the HL with elevated DOM fluorescence, extending down to approximately 250 m depth. Below the HL, waters mix with warmer and more saline AW with low DOM fluorescence. The other sections shown (ITP48 and ITP93) are from deployments in the Eurasian Arctic, capture the TPD with low salinity and very high DOM fluorescence in the surface 50 m, and also capture an underlying HL with DOM fluorescence intensity comparable to that seen in the Beaufort Sea HL (Figure 3).

3.1 Archetypical profiles

Figure 4a-c shows selected archetypical profiles for θ, S and DOM fluorescence in different basins. A profile in the western Nansen Basin (green) has characteristics typical of low DOM fluorescent AW entering the Arctic with surface waters being cooled and diluted by sea ice melt (Rudels et al., 2004). The winter mixed layer depth is apparent at around 100 m below which there is a coincident thermo-, halo- and DOM-clines. In this profile the winter mixed layer is capped by a surface lens with temperatures above freezing for its given salinity (Figure 4d, note deviation from freezing at salinity ~34), and reduced salinity and DOM fluorescence (Figure 4e) consistent with previous studies (Granskog et al., 2015; Williford et al., 2021). This likely reflects the addition of summer sea ice melt water (Bauch et al., 2011; Paffrath et al., 2021) into the surface layer. Sea-ice meltwater contributes with comparatively little DOM fluorescence (Granskog et al., 2015) and can be assumed to be low and comparable to that found in Atlantic waters (fluorescence <0.01 nm^{-1}). In this profile, the warm AW below has the highest temperature, salinity and DOM fluorescence, although the DOM fluorescence is very low (<0.01 nm^{-1}) in the upper water column and represents the “pure” AW before it accumulates any DOM signal on its path along the Arctic continental margin (Figure 1). For these waters highest DOM

fluorescence was measured at depth (deeper than 800m, measured using shipboard CTD), although still considerably lower than the surface DOM maxima from the other regions sampled.

In the profiles in the eastern Amundsen basin (magenta) and in the Makarov basin (black) (Figure 4a-c) the coincident thermo-, halo- and DOM-clines spanning from ~100 to 200m change character to cover greater range in salinity (S>34) and DOM fluorescence, and the direction of the DOM fluorescence gradient changes (now increasing with decreasing salinity) compared to in the Nansen basin. The temperature minimum is at around 50 m depth with temperatures very close to freezing (Figure 4d). Below the temperature minimum there is a distinct additional halocline extending to 100 m within which DOM fluorescence decreases essentially linearly with increasing salinity. This reveals that the correlation between DOM and salinity in these waters holds from the base of the PML (temperature minimum) to the AW (Figure 4d and e).

In the surface waters of the Amundsen and Makarov basins there is mixing of underlying halocline waters with ice meltwater. This is most evident for the Amundsen Basin profile (magenta) and at the very surface for the Makarov profile (black). The dilution acts to draw the data off the linear DOM-S mixing line (compare magenta and black profiles in Figure 4e) and towards a lower salinity and DOM fluorescence end member.

In Figure 4 two profiles from the Beaufort Gyre are shown (cyan and red). Although the depth distributions differ (Figure 4a-c), the water mass characteristics (S and DOM fluorescence in particular) of these two profiles overlap very closely (Figure 4d & e). The main deviation is in the surface 50 m with salinities below 32 where temperatures are considerably warmer in the profile that originates from closer to the Alaskan shelf (cyan) than in the central basin (red). In these profiles an additional thick upper layer of the UHC is evident underneath the PML, with salinities ranging from approximately 32 to 33. This layer has an intermediate DOM fluorescence which is less than half that found at comparable salinities in the Makarov Basin profile (black) but still much higher than that found in AW (green). The DOM-S diagram reveals that this layer sits above the LHC waters (Figure 4e).

In the region of the Alpha Ridge (Figure 4, blue), surface waters are diluted tending towards similar values for salinity and DOM fluorescence as that seen in the Beaufort Sea (Figure 4, red and cyan). Below this the water column have similar properties to the Makarov and Amundsen basin (black and magenta), with high DOM fluorescence and near freezing temperatures. At 90-150 m depth there is an intrusion of intermediate fluorescence DOM signal associated with UHC from the Beaufort Sea (Figure 4e).

For comparison, a profile from the East Greenland shelf (brown) is also shown in Figure 4. At salinities between 32 and 33 and at ~34.8 there is clear overlap in θ-S and DOM-S space with data from the central Arctic Ocean. Waters with these properties correspond to Beaufort Gyre upper halocline and Atlantic waters, respectively. But it should be noted this profile does not represent a widespread or typical signal for much of the East Greenland shelf. At other stations, not highlighted here, there are no overlap with the UHC waters but rather a more predominant signal from the Siberan shelf contribution (Amon et al., 2003; Gonçalves-Araujo et al., 2016).

3.2 DOM end member characteristics

The following present the results of an analysis of the properties and location of three distinct features in the profiles: the DOM fluorescence maximum, the temperature maximum and the temperature minimum. The analysis involves plotting histograms of these properties (Figure

5-7), which then reveal clear sub-groups of data. In order to determine the origins of the samples contributing to these groups, arbitrary distinctions are made depending on salinity, DOM fluorescence intensity or deviation from freezing temperature (see figure legends for boundaries of these arbitrary groups). The emphasis should be on the shape of the histograms (separate or overlapping distributions) and the grouping (colors) are just to facilitate interpretation.

Figure 5 shows histograms of water properties at the DOM fluorescence maxima for each profile for halocline waters (S 31-34). This reduces the data considerably and facilitates isolating the characteristics of different high intensity DOM sources, in particular in the range of halocline salinities across the Arctic. It is clear that DOM fluorescence maxima in the Arctic can be grouped into two based on their temperature (or rather deviation from freezing temperature, DFT): either essentially at seawater freezing temperatures (red group in Figure 5e) or centered around 0.4 °C above freezing (Figure 5e). The waters with the coldest (and closest to freezing) temperatures (red in Figure 5c) have the highest DOM fluorescence (>0.030 nm^{-1} with a tail extending up to 0.0888 nm^{-1}). Similarly, there is clear segregation with respect to depth. The DOM fluorescence maxima tend to be either at the surface (red group, with corresponding highest DOM fluorescence) or much deeper (between 100 and 250 m; Figure 5d) which is typically observed for the Beaufort Gyre stations (west of 100°W). The latter has lower DOM fluorescence centered around 0.03 nm^{-1} (blue and yellow data in Figure 5c).

The surface maxima (red) can also be segregated to maxima at depth <25m corresponding to profiles in the TPD, and maxima positioned just underneath the PML at approximately 60m (corresponding to the HL in the Eurasian Basin). These data span a range in salinities from 31 to 33.2 and originate from profiles taken in the Amundsen Basin, Lomonosov Ridge and near the North Pole. There is also a significant negative linear correlation between DOM fluorescence intensity and salinity for these samples ($r=-0.72$, $p<0.01$).

The lower CDOM intensity group (<0.030 nm^{-1}) could be segregated further into two, based on salinity, with a threshold between them of 33.2 (blue and yellow in Figure 5). Although there was a high degree of overlap in temperature (Figure 5b), typically ranging from 0.3 to 0.75 DFT, a two sample t-test indicated that there was a difference ($p<0.01$) with the higher salinity group (yellow) being significantly warmer. These groups also differed slightly in position in the water column, with the lower salinity group (blue) slightly shallower (mean depth 155 m) than the higher salinity group (mean depth 182 m, Figure 5d).

Another prominent feature of the water column in the Arctic is the intermediate and deep temperature maxima which traces the warm AW and Pacific waters that enter the Arctic (Jackson et al., 2010; Korhonen et al., 2013). In Figure 6 histograms of the properties of the temperature maximum are shown but binned based on their salinity and depth. For this analysis, only profiles where a distinct maximum was present are included (i.e., shallow ITP profiles (~200 m) where temperature was still increasing with depth were not included). Here one can identify three groups with contrasting in θ, S and DOM fluorescence (Figure 6). The AW inflow temperature maximum waters (shown in blue) are widespread across the basin at depths between 200 and 350 m, S of ~34.9, temperatures ranging between 0.5 and 2 °C and have low DOM fluorescence (~0.01 nm^{-1}). In the Canada Basin, salinity at deep (AW) temperature maximum(0.7-0.9 °C), is slightly lower (34.8), but has comparably low DOM fluorescence of ~0.01 nm^{-1} (shown in yellow). This water is found deeper in the water column (350-400 m). The final group, shown in red, corresponds to near surface waters in the Canada Basin that have entered from Pacific, and experienced warming and sea ice melt. These waters have comparatively higher DOM fluorescence, centered around 0.017 nm^{-1}.

An analysis of the properties of the temperature minimum also revealed clear groups based on temperature and salinity (Figure 7). The deep temperature minimum (typically >100 m) in the Canada Basin differed from the others by having temperatures that deviated more than 0.2 °C from seawater freezing (blue) and DOM fluorescence of 0.028 nm^{-1}. In surface waters the temperature minima were largely within 0.2 °C from seawater freezing but could be segregated based on salinity. The lowest salinity temperature minimum (S<29) was restricted to very surface waters and the majority of the data had low DOM fluorescence (<0.012 nm^{-1}). At salinities between 29.5 and 32 two distinct groups could be identified, lower salinity group with low DOM fluorescence (~0.02 nm^{-1}, S 30-31) and a higher salinity group with the higher DOM fluorescence (~0.03 nm^{-1}, S32-33). Both these were at depths between 40-70 m

4 Discussion

Figure 8 shows the average properties of each of the identified end members from the DOM and temperature maxima and temperature minima, superimposed on all the data in θ-S and DOM-S space. From this one can see that the DOM fluorescence signal offers an additional parameter from which to separate the properties of Arctic surface waters (S<34 and θ<0), where temperatures are often low and overlap considerably despite different water mass origins. In particular the data can resolve patterns in the UHC while the differences in the DOM fluorescence of AW as it propagates into the Arctic are minor.

4.1 Oceanic DOM signal associated with AW branches.

The DOM fluorescence signal found in the temperature maximum waters originating from AW has comparable intensity to that found in earlier studies for ocean waters without a notable influence from terrestrial input (Jørgensen et al., 2011; Zabłocka et al., 2020). This represents a background recalcitrant oceanic signal produced from the long term microbial and photochemical processing of marine organic matter in the world ocean (Jørgensen et al., 2011, 2014; Yamashita & Tanoue, 2008). AW enters the Arctic through the Fram Strait or via the Barents Sea (Rudels et al., 2004).

The Fram Strait and Barents Sea contributions to these surface waters are cooled and diluted by sea ice melt. This has a diluting effect on the ocean DOM fluorescence signal brought with it as seen for the Nansen Basin profile in Figure 4. These waters flow eastwards along the Siberian continental slope forming the Arctic Circumpolar Boundary Current (ACBC) (Aksenov et al., 2011). The saline temperature maximum endmembers identified in Figure 6 likely trace the path of AW starting shallow (200-350 m) and with variable warm temperatures in the Eurasian Basin (0.5-2 C) and ending as a deeper (400-500m) cooler temperature maxima (0.7-0.9 C) in the Canada Basin which is more homogenous with respect to temperature and only slightly less saline (S 34.8). The DOM fluorescence in these waters does not change reflecting the common AW origins and indicating little influence from riverine or shelf sediment organic matter inputs. This has also been confirmed earlier using terrestrial plant biomarker lignin measurements (Kaiser et al., 2017).

The waters of the LHC are defined as having salinities greater than 34 and temperatures below 0 C (Korhonen et al., 2013; Rudels et al., 1996). These originate from the freshening and cooling of AW after entering the Arctic north of Svalbard or via the Barents Sea. As a result, one would expect them to have a very low DOM fluorescence (as discussed above). The majority of the water sampled with a salinity greater than 34 had higher DOM fluorescence than expected for AW, 0.03 nm^{-1} rather than 0.01 nm^{-1}, (Figure 8) and was positioned on the Siberian shelf –

AW mixing line. Two regions are thought to contribute to the formation of the LHC, and these results imply that the open ocean convective contribution to the LHC from winter waters in the Nansen Basin (Rudels et al., 1996) may be of minor importance in the waters sampled here. The clear elevated DOM fluorescence emphasizes the importance of the Barents Sea branch entering via the Kara Sea where there is a terrestrial DOM contribution from Siberian rivers. Almost all of the Atlantic-derived water beyond the Lomonosov Ridge is thought to have come through the Barents Sea (B. Rudels et al., 1996) but the data here indicate a dominance of this water also on the Eurasian side with little evidence for the other branch.

4.2 Shelf DOM signals

A branch of the Barents Sea supply of AW contains a contribution from the Norwegian Coastal Current and flows along the Siberian shelf and slope (Osadchiev et al., 2020; Rudels et al., 2004). During this passage it collects freshwater (Bauch et al., 2014) and DOM from Siberian rivers (Kaiser et al., 2017). Export of these waters northwards off the shelf and mixing with underlying AW results in the negative correlation observed between DOM fluorescence and salinity (e.g., black profile in Figure 4). The end member analysis of the DOM fluorescence maxima identified three distinct groups with shelf origins and demonstrates that different shelf components are detectable in the HL as has been demonstrated based on Nd isotopes for the Lapev and Kara seas components within the TPD (Paffrath et al., 2021). The group with the highest DOM fluorescence values (red in Figure 5) overlap in salinity, temperature and depth with previously defined Lower Salinity Halocline Waters (LSHW) (Bauch et al., 2014; Dorothea Bauch et al., 2011). These waters originate from the Laptev and East Siberian Seas (Bauch et al., 2014) and are exported northwards off shelf forming the surface waters of the TPD (Rudels et al., 1999) and carry with them a high terrigenous DOM fluorescence (Charette et al., 2020). DOM fluorescence at salinities of 30 for shelf waters near the Lena River have been reported to be around 0.1 nm^{-1} (Gonçalves-Araujo et al., 2015) and this aligns well if one extrapolates the mixing curve for the Makarov Basin (black) shown in Figure 4. Measurement of the terrestrial plant biomarker lignin has also shown that the DOM in these waters originates from the Ob, Yenisei and Lena rivers (Kaiser et al., 2017). The strong linear correlation with salinity indicates conservative mixing between LSHW of the TPD with the underlying AW of the temperature maximum. The results also show that in places (Canada Basin side of TDP) this can be subducted under a lower salinity surface water from the Beaufort Sea (Figure 4, blue; Figure 5, red).

LSHW temperatures are very close to freezing, which (for the most part within 0.3 °C of freezing for their given salinity) confirms the role that brine release during sea ice formation has on shaping the properties of these waters (Aagaard et al., 1981). Mixing with ice melt water is apparent in the very surface waters of the profiles where both DOM fluorescence and salinity is reduced (black profile in Figure 4) and is consistent with a recent study with extensive coverage of the Siberian shelf water (Hölemann et al., 2021).

The highest salinity DOM fluorescence maximum end member (S 33.7, Figure 8) lies on the same LSHW–AW mixing line, but is found at depths greater than 150 m, and slightly warmer (yellow in Figure 5). The fact that this end member lies directly on this mixing line hints to the fact that it is also formed on the Siberian shelf but contains a greater contribution of Atlantic water. Although salinities range between 33.4-34.2, its depth and location indicates that it represents part of the LHC in the Canada Basin.

A third end member with similar DOM fluorescence but lower salinities (mean S 32.9) was also identified (blue in Figure 5). These waters also have warmer temperatures,

approximately 0.4 °C above seawater freezing, and represent Pacific inflow waters which have accumulated DOM whilst passing across the Chuckchi Sea (Jones & Anderson, 1986; Stedmon et al., 2011). This is confirmed by the fact that near identical water column characteristics can be found in the Chuckchi Sea and the Beaufort Sea profiles (compare red and cyan data in Figure 4). As Pacific waters pass over the shelf, seasonal sea-ice formation (Shimada, 2005) acts to drive temperatures close to freezing and there is a DOM contribution from marine organic matter degradation in shelf sediments. Here the DOM released clearly differs in character from riverine material and likely originated from the degradation of marine organic matter (Stedmon et al., 2011). This aligns with the nutrient signal reported for these waters (Jones & Anderson, 1986, p. 198). In the Canada Basin, these waters lie on top of LHC from the Eurasian Basin (red and cyan data in Figure 3) however in the region of the Alpha Ridge (blue profile in Figure 3) one can find contribution from all three DOM endmembers with Chuckchi shelf UHC water inserted between LSHW and LHC. This fits with earlier observations in the central Arctic (McLaughlin et al., 2004; Shimada, 2005; Woodgate et al., 2007) and from the Wandel Sea off Northeast Greenland (Dmitrenko et al., 2019). Waters with the same properties, overlapping in θ-S and DOM-S space, were also identified by the analysis of the temperature minimum (Figure 8, blue and lack points at S of ~33). The temperature and salinity confirms its origin as PWW.

The shallow temperature maximum <100m in the Canada Basin represents the Pacific inflow as PSW (Rudels et al., 2004). This was distinguished as a group of data with salinities between 30 and 32 and intermediate DOM fluorescence (red in Figure 8). The location of these data in DOM-S space indicate that they represent a dilution of the PWW, with an accumulated contribtion of freshwater from ice melt.

Figure 9 summarizes the patterns reported in the distribution of DOM fluorescence. At the surface low salinity (S<32.5) and high DOM fluorescence waters (LSHW) that originate on the Siberian shelf and are exported northwards with the TPD. Below this are the waters of the Atlantic derived LHC which have intermediate DOM fluorescence indicating that they have also entrained terrestrial DOM from the Siberian shelf during their formation before exported northwards. In addition to being exported northwards together with the TPD they are also diverted into the Beaufort Sea where they transfer terrestrial DOM into the LHC beneath the UHC. The UHL, despite having comparable DOM fluorescence to the LHC, have a lower salinity and collects its (marine) DOM signal from the Chuckchi shelf. All three components of HL are exported across the pole to the Fram Strait. While the signal at the surface from the TPD is likely lost due to dilution with glacial and sea ice melt on its journey out of the Arctic, the signals from the Pacific and Atlantic HL at depth are retained and identifiable all the way to the East Greenland shelf. This is supported by comparing the data collected from the Beaufort Sea (cyan and red, Figure 4e) with measurements from the East Greenland Shelf in DOM-S space (brown, Figure 4e), and supports earlier evidence based on water samples (Gonçalves-Araujo et al., 2016).

5 Conclusions

5.1 Perspectives of DOM measurements from automated platforms

The results shown indicate that two major freshwater sources to the Arctic, river discharge and Pacific water, have clear and distinguishable DOM fluorescence signals associated with them. This confirms earlier findings based on more in-depth water sample analysis (Amon et al, 2003;

Gonçalves-Araujo et al., 2016; Stedmon et al., 2011) but here the high spatial resolution of in situ measurements complements the increased analytical resolution of laboratory measurements.

DOM fluorescence at the wavelengths measured by these sensors (UVA excitation and visible wavelength fluorescence), behaves largely conservatively with salinity during sea ice formation and subsequent brine rejection (Stedmon et al., 2011). The released brine (with slightly elevated salinities and DOM fluorescence, and near seawater freezing temperatures) contributes to the formation of shelf waters that feed the HL. While Siberian shelf water contribute with terrestrial DOM into the LHC, the water from the Chuckchi shelf contribute with marine DOM likely released from sediment below highly productive water. Despite the fact that the high salinity waters of the LHC are thought to contain a contribution from winter mixing in the Nansen Basins, the evidence shown here indicates widespread dominance of shelf water source.

In the upper 300m of the Beaufort Gyre salinity profiles reflect the considerable storage of freshwater in the region. Here DOM profiles from automated platforms may provide additional insight to the source of the freshwater. River water and Pacific water will be associated with high DOM fluorescence while accumulation of sea-ice melt will dilute DOM fluorescence (resulting in positive correlation with salinity). The DOM fluorescence-S diagrams clearly show an accumulation of sea-ice melt in the surface 50 m (salinities below 30). Combination with additional biogeochemical sensors such as nitrate and oxygen (Athanase et al., 2019), will provide an opportunity to fractionate freshwater contributions based on in situ measurements alone. Surface DOM measurements can easily distinguish the frontal regions either side of the TPD, and in the vertical provides a powerful tool to guide water sampling of other tracers in the water column. This offers a valuable and currently underutilized additional tracer for deciphering Arctic circulation and freshwater distribution.

Acknowledgments, Samples, and Data

Danish Strategic Research Council for the NAACOS project (grant no. 10-093903), the Danish Center for Marine Research (grant no. 2012-01). C. A. S. has received funding from the Independent Research Fund Denmark Grant No. 9040−00266B. Deployment and recovery of ITP93 and sampling at PS94 was done within the Helmholtz Infrastructure Initiative FRAM ("Frontiers of Arctic Marine Monitoring"). We thank the FRAM associated technicians, engineers, and administrators as well as the captains, crews, and chief scientists of the cruises who were all instrumental in making these observations possible. RG−A has received funding from the European Union's Horizon 2020 research and innovation program under the Marie Skłodowska−Curie Grant Agreement No. 839311. The complete dataset is available for download from PANGEA at (link to come).

References

Aagaard, K., Coachman, L. K., & Carmack, E. (1981). On the halocline of the Arctic Ocean. *Deep Sea Research Part A. Oceanographic Research Papers*, *28*(6), 529–545. https://doi.org/10.1016/0198-0149(81)90115-1

561 Aksenov, Y., Ivanov, V. V., Nurser, A. J. G., Bacon, S., Polyakov, I. V., Coward, A. C., et al.
562 (2011). The Arctic Circumpolar Boundary Current. *Journal of Geophysical Research:*
563 *Oceans*, *116*(C9). https://doi.org/10.1029/2010JC006637
564 Amon, Rainer M. W., Budéus, G. Meon, B. (2003). Dissolved organic carbon distribution and
565 origin in the Nordic Seas: Exchanges with the Arctic Ocean and the North Atlantic.
566 *Journal of Geophysical Research*, *108*(C7). https://doi.org/10.1029/2002JC001594
567 Amon, R.M.W., Rinehart, A. J., Duan, S., Louchouarn, P., Prokushkin, A., Guggenberger, G., et
568 al. (2012). Dissolved organic matter sources in large Arctic rivers. *Geochimica et*
569 *Cosmochimica Acta*, *94*, 217–237. https://doi.org/10.1016/j.gca.2012.07.015
570 Anderson, L. G., & Amon, R. M. W. (2015). DOM in the Arctic Ocean. In *Biogeochemistry of*
571 *Marine Dissolved Organic Matter* (pp. 609–633). Elsevier. https://doi.org/10.1016/B978-
572 0-12-405940-5.00014-5
573 Anderson, L. G., Andersson, P. S., Björk, G., Peter Jones, E., Jutterström, S., & Wåhlström, I.
574 (2013). Source and formation of the upper halocline of the Arctic Ocean: ARCTIC
575 OCEAN UPPER HALOCLINE. *Journal of Geophysical Research: Oceans*, *118*(1), 410–
576 421. https://doi.org/10.1029/2012JC008291
577 Athanase, M., Sennéchael, N., Garric, G., Koenig, Z., Boles, E., & Provost, C. (2019). New
578 Hydrographic Measurements of the Upper Arctic Western Eurasian Basin in 2017 Reveal
579 Fresher Mixed Layer and Shallower Warm Layer Than 2005–2012 Climatology. *Journal*
580 *of Geophysical Research: Oceans*, *124*(2), 1091–1114.
581 https://doi.org/10.1029/2018JC014701
582 Bauch, D., Torres-Valdes, S., Polyakov, I., Novikhin, A., Dmitrenko, I., McKay, J., & Mix, A.
583 (2014). Halocline water modification and along-slope advection at the Laptev Sea

584 continental margin. *Ocean Science*, *10*(1), 141–154. https://doi.org/10.5194/os-10-141-
585 2014
586 Bauch, Dorothea, van der Loeff, M. R., Andersen, N., Torres-Valdes, S., Bakker, K., &
587 Abrahamsen, E. P. (2011). Origin of freshwater and polynya water in the Arctic Ocean
588 halocline in summer 2007. *Progress in Oceanography*, *91*(4), 482–495.
589 https://doi.org/10.1016/j.pocean.2011.07.017
590 Belzile, C., Roesler, C. S., Christensen, J. P., Shakhova, N., & Semiletov, I. (2006). Fluorescence
591 measured using the WETStar DOM fluorometer as a proxy for dissolved matter
592 absorption. *Estuarine, Coastal and Shelf Science*, *67*(3), 441–449.
593 https://doi.org/10.1016/j.ecss.2005.11.032
594 Bertosio, C., Provost, C., Sennéchael, N., Artana, C., Athanase, M., Boles, E., et al. (2020). The
595 Western Eurasian Basin Halocline in 2017: Insights From Autonomous NO
596 Measurements and the Mercator Physical System. *Journal of Geophysical Research:*
597 *Oceans*, *125*(7), e2020JC016204. https://doi.org/10.1029/2020JC016204
598 Boles, E., Provost, C., Garçon, V., Bertosio, C., Athanase, M., Koenig, Z., & Sennéchael, N.
599 (2020). Under-Ice Phytoplankton Blooms in the Central Arctic Ocean: Insights From the
600 First Biogeochemical IAOOS Platform Drift in 2017. *Journal of Geophysical Research:*
601 *Oceans*, *125*(3), e2019JC015608. https://doi.org/10.1029/2019JC015608
602 Charette, M. A., Kipp, L. E., Jensen, L. T., Dabrowski, J. S., Whitmore, L. M., Fitzsimmons, J.
603 N., et al. (2020). The Transpolar Drift as a Source of Riverine and Shelf-Derived Trace
604 Elements to the Central Arctic Ocean. *Journal of Geophysical Research: Oceans*, *125*(5),
605 e2019JC015920. https://doi.org/10.1029/2019JC015920

606 Chen, M., Kim, J.-H., Nam, S.-I., Niessen, F., Hong, W.-L., Kang, M.-H., & Hur, J. (2016).
607 Production of fluorescent dissolved organic matter in Arctic Ocean sediments. *Scientific*
608 *Reports*, *6*(1), 39213. https://doi.org/10.1038/srep39213
609 Coachman, L. K., & Aagaard, K. (1974). Physical Oceanography of Arctic and Subarctic Seas.
610 In Y. Herman (Ed.), *Marine Geology and Oceanography of the Arctic Seas* (pp. 1–72).
611 Berlin, Heidelberg: Springer. https://doi.org/10.1007/978-3-642-87411-6_1
612 Coachman, L. K., & Barnes, C. A. (1961). The Contribution of Bering Sea Water to the Arctic
613 Ocean. *Arctic*, *14*(3), 147–161.
614 Codispoti, L. A., Flagg, C., Kelly, V., & Swift, J. H. (2005). Hydrographic conditions during the
615 2002 SBI process experiments. *Deep Sea Research Part II: Topical Studies in*
616 *Oceanography*, *52*(24–26), 3199–3226. https://doi.org/10.1016/j.dsr2.2005.10.007
617 Cooper, L. W., Benner, R., McClelland, J. W., Peterson, B. J., Holmes, R. M., Raymond, P. A.,
618 et al. (2005). Linkages among runoff, dissolved organic carbon, and the stable oxygen
619 isotope composition of seawater and other water mass indicators in the Arctic Ocean:
620 ARCTIC RUNOFF, DOC, AND OXYGEN ISOTOPES. *Journal of Geophysical*
621 *Research: Biogeosciences*, *110*(G2), n/a-n/a. https://doi.org/10.1029/2005JG000031
622 Dmitrenko, I. A., Kirillov, S. A., Ivanov, V. V., Woodgate, R. A., Polyakov, I. V., Koldunov, N.,
623 et al. (2009). Seasonal modification of the Arctic Ocean intermediate water layer off the
624 eastern Laptev Sea continental shelf break. *Journal of Geophysical Research: Oceans*,
625 *114*(C6). https://doi.org/10.1029/2008JC005229
626 Dmitrenko, I. A., Ivanov, V. V., Kirillov, S. A., Vinogradova, E. L., Torres−Valdes, S., &
627 Bauch, D. (2011). Properties of the Atlantic derived halocline waters over the Laptev Sea

628 continental margin: Evidence from 2002 to 2009. *Journal of Geophysical Research:*
629 *Oceans*, *116*(C10). https://doi.org/10.1029/2011JC007269
630 Dmitrenko, I. A., Kirillov, S. A., Rudels, B., Babb, D. G., Myers, P. G., Stedmon, C. A., et al.
631 (2019). Variability of the Pacific-Derived Arctic Water Over the Southeastern Wandel
632 Sea Shelf (Northeast Greenland) in 2015-2016. *Journal of Geophysical Research:*
633 *Oceans*. https://doi.org/10.1029/2018JC014567
634 Gonçalves-Araujo, R., Stedmon, C. A., Heim, B., Dubinenkov, I., Kraberg, A., Moiseev, D., &
635 Bracher, A. (2015). From Fresh to Marine Waters: Characterization and Fate of
636 Dissolved Organic Matter in the Lena River Delta Region, Siberia. *Frontiers in Marine*
637 *Science*, *2*. https://doi.org/10.3389/fmars.2015.00108
638 Gonçalves-Araujo, R., Granskog, M. A., Bracher, A., Azetsu-Scott, K., Dodd, P. A., & Stedmon,
639 C. A. (2016). Using fluorescent dissolved organic matter to trace and distinguish the
640 origin of Arctic surface waters. *Scientific Reports*, *6*(1).
641 https://doi.org/10.1038/srep33978
642 Granskog, M. A., Pavlov, A. K., Sagan, S., Kowalczuk, P., Raczkowska, A., & Stedmon, C. A.
643 (2015). Effect of sea-ice melt on inherent optical properties and vertical distribution of
644 solar radiant heating in Arctic surface waters: EFFECT OF ICE MELT ON SOLAR
645 HEATING. *Journal of Geophysical Research: Oceans*, *120*(10), 7028–7039.
646 https://doi.org/10.1002/2015JC011087
647 Haine, T. W. N., Curry, B., Gerdes, R., Hansen, E., Karcher, M., Lee, C., et al. (2015). Arctic
648 freshwater export: Status, mechanisms, and prospects. *Global and Planetary Change*,
649 *125*, 13–35. https://doi.org/10.1016/j.gloplacha.2014.11.013

650 Hardison, A. K., McTigue, N. D., Gardner, W. S., & Dunton, K. H. (2017). Arctic shelves as
651 platforms for biogeochemical activity: Nitrogen and carbon transformations in the
652 Chukchi Sea, Alaska. *Deep Sea Research Part II: Topical Studies in Oceanography*, *144*,
653 78–91. https://doi.org/10.1016/j.dsr2.2017.08.004
654 Hölemann, J. A., Juhls, B., Bauch, D., Janout, M., Koch, B. P., & Heim, B. (2021). The impact
655 of land-fast ice on the distribution of terrestrial dissolved organic matter in the Siberian
656 Arctic shelf seas. *Biogeosciences Discussions*, 1–30. https://doi.org/10.5194/bg-2020-462
657 Holmes, R. M., McClelland, J. W., Peterson, B. J., Tank, S. E., Bulygina, E., Eglinton, T. I., et
658 al. (2012). Seasonal and Annual Fluxes of Nutrients and Organic Matter from Large
659 Rivers to the Arctic Ocean and Surrounding Seas. *Estuaries and Coasts*, *35*(2), 369–382.
660 https://doi.org/10.1007/s12237-011-9386-6
661 Jackson, J. M., Carmack, E. C., McLaughlin, F. A., Allen, S. E., & Ingram, R. G. (2010).
662 Identification, characterization, and change of the near-surface temperature maximum in
663 the Canada Basin, 1993–2008. *Journal of Geophysical Research: Oceans*, *115*(C5).
664 https://doi.org/10.1029/2009JC005265
665 Jones, E. P., & Anderson, L. G. (1986). On the origin of the chemical properties of the Arctic
666 Ocean halocline. *Journal of Geophysical Research*, *91*(C9), 10759.
667 https://doi.org/10.1029/JC091iC09p10759
668 Jørgensen, L., Stedmon, C. A., Kragh, T., Markager, S., Middelboe, M., & Søndergaard, M.
669 (2011). Global trends in the fluorescence characteristics and distribution of marine
670 dissolved organic matter. *Marine Chemistry*, *126*(1–4), 139–148. https://doi.org/10.1016/
671 j.marchem.2011.05.002

672 Jørgensen, L., Stedmon, C. A., Granskog, M. A., & Middelboe, M. (2014). Tracing the long-term
673 microbial production of recalcitrant fluorescent dissolved organic matter in seawater:
674 MIDDELBOE ET. AL.; MICROBIAL PRODUCTION OF RECALCITRANT DOM.
675 *Geophysical Research Letters*, *41*(7), 2481–2488. https://doi.org/10.1002/2014GL059428
676 Kaiser, K., Benner, R., & Amon, R. M. W. (2017). The fate of terrigenous dissolved organic
677 carbon on the Eurasian shelves and export to the North Atlantic: ARCTIC
678 TERRIGENOUS DOC REMOVAL. *Journal of Geophysical Research: Oceans*, *122*(1),
679 4–22. https://doi.org/10.1002/2016JC012380
680 Korhonen, M., Rudels, B., Marnela, M., Wisotzki, A., & Zhao, J. (2013). Time and space
681 variability of freshwater content, heat content and seasonal ice melt in the Arctic Ocean
682 from 1991 to 2011. *Ocean Science*, *9*(6), 1015–1055. https://doi.org/10.5194/os-9-1015-
683 2013
684 Krishfield, R., Toole, J., Proshutinsky, A., & Timmermans, M.-L. (2008). Automated Ice-
685 Tethered Profilers for Seawater Observations under Pack Ice in All Seasons. *Journal of*
686 *Atmospheric and Oceanic Technology*, *25*(11), 2091–2105.
687 https://doi.org/10.1175/2008JTECHO587.1
688 Laney, S. R., Krishfield, R. A., Toole, J. M., Hammar, T. R., Ashjian, C. J., & Timmermans, M.-
689 L. (2014). Assessing algal biomass and bio-optical distributions in perennially ice-
690 covered polar ocean ecosystems. *Polar Science*, *8*(2), 73–85.
691 https://doi.org/10.1016/j.polar.2013.12.003
692 Lawaetz, A. J., & Stedmon, C. A. (2009). Fluorescence intensity calibration using the Raman
693 scatter peak of water. *Applied Spectroscopy*, *63*(8), 936–940.
694 https://doi.org/10.1366/000370209788964548.

695 Makarewicz, A., Kowalczuk, P., Sagan, S., Granskog, M. A., Pavlov, A. K., Zdun, A., et al.
696 (2018). Characteristics of chromophoric and fluorescent dissolved organic matter in the
697 Nordic Seas. *Ocean Science*, *14*(3), 543–562. https://doi.org/10.5194/os-14-543-2018
698 McLaughlin, F. A., Carmack, E. C., Macdonald, R. W., Melling, H., Swift, J. H., Wheeler, P. A.,
699 et al. (2004). The joint roles of Pacific and Atlantic-origin waters in the Canada Basin,
700 1997–1998. *Deep Sea Research Part I: Oceanographic Research Papers*, *51*(1), 107–
701 128. https://doi.org/10.1016/j.dsr.2003.09.010
702 Morison, J., Kwok, R., Peralta-Ferriz, C., Alkire, M., Rigor, I., Andersen, R., & Steele, M.
703 (2012). Changing Arctic Ocean freshwater pathways. *Nature*, *481*(7379), 66–70.
704 https://doi.org/10.1038/nature10705
705 Murphy, K. R., Butler, K. D., Spencer, R. G. M., Stedmon, C. A., Boehme, J. R., & Aiken, G. R.
706 (2010). Measurement of Dissolved Organic Matter Fluorescence in Aquatic
707 Environments: An Interlaboratory Comparison. *Environmental Science & Technology*,
708 *44*(24), 9405–9412. https://doi.org/10.1021/es102362t
709 Osadchiev, A. A., Pisareva, M. N., Spivak, E. A., Shchuka, S. A., & Semiletov, I. P. (2020).
710 Freshwater transport between the Kara, Laptev, and East-Siberian seas. *Scientific*
711 *Reports*, *10*(1), 13041. https://doi.org/10.1038/s41598-020-70096-w
712 Overeem, I., & Syvitski, J. P. M. (2010). Shifting discharge peaks in arctic rivers, 1977–2007.
713 *Geografiska Annaler: Series A, Physical Geography*, *92*(2), 285–296.
714 https://doi.org/10.1111/j.1468-0459.2010.00395.x
715 Peralta-Ferriz, C., & Woodgate, R. A. (2015). Seasonal and interannual variability of pan-Arctic
716 surface mixed layer properties from 1979 to 2012 from hydrographic data, and the

717 dominance of stratification for multiyear mixed layer depth shoaling. *Progress in*
718 *Oceanography*, *134*, 19–53. https://doi.org/10.1016/j.pocean.2014.12.005
719 Peterson, B. J., Holmes, R. M., McClelland, J. W., Vörösmarty, C. J., Lammers, R. B.,
720 Shiklomanov, A. I., et al. (2002). Increasing River Discharge to the Arctic Ocean.
721 *Science*, *298*(5601), 2171–2173. https://doi.org/10.1126/science.1077445
722 Polyakov, I. V., Rippeth, T. P., Fer, I., Alkire, M. B., Baumann, T. M., Carmack, E. C., et al.
723 (2020). Weakening of Cold Halocline Layer Exposes Sea Ice to Oceanic Heat in the
724 Eastern Arctic Ocean. *Journal of Climate*, *33*(18), 8107–8123.
725 https://doi.org/10.1175/JCLI-D-19-0976.1
726 Rabe, B., Schauer, U., Ober, S., Horn, M., Hoppmann, M., Korhonen, M., et al. (2016a).
727 Physical oceanography during POLARSTERN cruise PS94 (ARK-XXIX/3) [Data set].
728 *Alfred Wegener Institute, Helmholtz Centre for Polar and Marine Research,*
729 *Bremerhaven*. PANGAEA. https://doi.org/10.1594/PANGAEA.859558
730 Rabe, B., Schauer, U., Ober, S., Horn, M., Hoppmann, M., Korhonen, M., et al. (2016b, April
731 13). Physical oceanography measured on water bottle samples during POLARSTERN
732 cruise PS94 (ARK-XXIX/3). *Alfred Wegener Institute, Helmholtz Centre for Polar and*
733 *Marine Research, Bremerhaven*. PANGAEA.
734 https://doi.org/10.1594/PANGAEA.859559
735 Rudels, B., Anderson, L. G., & Jones, E. P. (1996). Formation and evolution of the surface
736 mixed layer and halocline of the Arctic Ocean. *Journal of Geophysical Research:*
737 *Oceans*, *101*(C4), 8807–8821. https://doi.org/10.1029/96JC00143

738 Rudels, Bert, J. Friedrich, H., & Quadfasel, D. (1999). The Arctic Circumpolar Boundary
739 Current. *Deep Sea Research Part II: Topical Studies in Oceanography*, *46*(6), 1023–
740 1062. https://doi.org/10.1016/S0967-0645(99)00015-6
741 Rudels, Bert, Muench, R. D., Gunn, J., Schauer, U., & Friedrich, H. J. (2000). Evolution of the
742 Arctic Ocean boundary current north of the Siberian shelves. *Journal of Marine Systems*,
743 *25*(1), 77–99. https://doi.org/10.1016/S0924-7963(00)00009-9
744 Rudels, Bert, Jones, E. P., Schauer, U., & Eriksson, P. (2004). Atlantic sources of the Arctic
745 Ocean surface and halocline waters. *Polar Research*, *32*(2), 181–208.
746 Serreze, M. C., Barrett, A. P., Slater, A. G., Woodgate, R. A., Aagaard, K., Lammers, R. B., et
747 al. (2006). The large-scale freshwater cycle of the Arctic. *Journal of Geophysical*
748 *Research*, *111*(C11). https://doi.org/10.1029/2005JC003424
749 Shimada, K. (2005). Halocline structure in the Canada Basin of the Arctic Ocean. *Geophysical*
750 *Research Letters*, *32*(3). https://doi.org/10.1029/2004GL021358
751 Stedmon, C. A., Thomas, D. N., Papadimitriou, S., Granskog, M. A., & Dieckmann, G. S.
752 (2011). Using fluorescence to characterize dissolved organic matter in Antarctic sea ice
753 brines. *Journal of Geophysical Research*, *116*(G3).
754 https://doi.org/10.1029/2011JG001716
755 Stedmon, C.A., Amon, R. M. W., Rinehart, A. J., & Walker, S. A. (2011). The supply and
756 characteristics of colored dissolved organic matter (CDOM) in the Arctic Ocean: Pan
757 Arctic trends and differences. *Marine Chemistry*, *124*(1–4), 108–118.
758 https://doi.org/10.1016/j.marchem.2010.12.007

759 Stedmon, C. A., & Cory, R. M. (2014). Biological origins and fate of fluorescent dissolved
760 organic matter in aquatic environments. *Aquatic Organic Matter Fluorescence*, 278–299.
761 https://doi.org/10.1017/CBO9781139045452.013
762 Stedmon, C. A., & Nelson, N. B. (2015). The Optical Properties of DOM in the Ocean. In
763 *Biogeochemistry of Marine Dissolved Organic Matter* (pp. 481–508). Elsevier.
764 https://doi.org/10.1016/B978-0-12-405940-5.00010-8
765 Steele, M., & Boyd, T. (1998). Retreat of the cold halocline layer in the Arctic Ocean. *Journal of*
766 *Geophysical Research: Oceans*, *103*(C5), 10419–10435.
767 https://doi.org/10.1029/98JC00580
768 Steele, M., Morison, J., Ermold, W., Rigor, I., Ortmeyer, M., & Shimada, K. (2004). Circulation
769 of summer Pacific halocline water in the Arctic Ocean. *Journal of Geophysical Research:*
770 *Oceans*, *109*(C2). https://doi.org/10.1029/2003JC002009
771 Timmermans, M.-L., Toole, J., & Krishfield, R. (2018). Warming of the interior Arctic Ocean
772 linked to sea ice losses at the basin margins. *Science Advances*, *4*(8), eaat6773.
773 https://doi.org/10.1126/sciadv.aat6773
774 Toole, J., Krishfield, R., Timmermans, M.-L., & Proshutinsky, A. (2011). The Ice-Tethered
775 Profiler: Argo of the Arctic. *Oceanography*, *24*(3), 126–135.
776 https://doi.org/10.5670/oceanog.2011.64
777 Toole, J. M., Timmermans, M.-L., Perovich, D. K., Krishfield, R. A., Proshutinsky, A., &
778 Richter−Menge, J. A. (2010). Influences of the ocean surface mixed layer and
779 thermohaline stratification on Arctic Sea ice in the central Canada Basin. *Journal of*
780 *Geophysical Research: Oceans*, *115*(C10). https://doi.org/10.1029/2009JC005660

781 Toole, J. M., Krishfield, R., & Woods Hole Oceanographic Institution Ice-Tethered Profiler
782 Program. (2016). Ice-Tethered Profiler observations: Vertical profiles of temperature,
783 salinity, oxygen, and ocean velocity from an Ice-Tethered Profiler buoy system [Data
784 set]. NOAA National Centers for Environmental Information.
785 https://doi.org/10.7289/V5MW2F7X
786 Williford, T., Amon, R. M. W., Benner, R., Kaiser, K., Bauch, D., Stedmon, C., et al. (2021).
787 Insights into the origins, molecular characteristics and distribution of iron-binding ligands
788 in the Arctic Ocean. *Marine Chemistry*, *231*, 103936.
789 https://doi.org/10.1016/j.marchem.2021.103936
790 Woodgate, R. A., Aagaard, K., Swift, J. H., Smethie, W. M., & Falkner, K. K. (2007). Atlantic
791 water circulation over the Mendeleev Ridge and Chukchi Borderland from thermohaline
792 intrusions and water mass properties. *Journal of Geophysical Research: Oceans*,
793 *112*(C2). https://doi.org/10.1029/2005JC003416
794 Yamashita, Y., & Tanoue, E. (2008). Production of bio-refractory fluorescent dissolved organic
795 matter in the ocean interior. *Nature Geoscience*, *1*(9), 579–582.
796 https://doi.org/10.1038/ngeo279
797 Zabłocka, M., Kowalczuk, P., Meler, J., Peeken, I., Dragańska-Deja, K., & Winogradow, A.
798 (2020). Compositional differences of fluorescent dissolved organic matter in Arctic
799 Ocean spring sea ice and surface waters north of Svalbard. *Marine Chemistry*, *227*,
800 103893. https://doi.org/10.1016/j.marchem.2020.103893
801

802

803 **Figure 1**. ITP drift pathways, cruise stations and schematic of general circulation pathways. Red
804 arrow indicate inflowing ocean water; Blue arrows polar water exiting Arctic, Light-blue major
805 Arctic rivers. Black indicates two features of the central Arctic, Transpolar drift extending from
806 shelf and passing over the pole, and the Beaufort Gyre. Solid and dotted lines indicate position of
807 these under positive and negative Arctic Oscillation (Morison et al 2012). Legend indicates the
808 ITP and cruise identity. The numbers on the map indicate areas: 1) Nansen Basin; 2) Gakkel
809 Ridge; 3) Amundsen Basin; 4) Lomonosov Ridge; 5) Makarov Basin; 6) Alpha Ridge; 7)
810 Mendelev Ridge; 8 Beaufort Sea; 9 Chukchi Plateau; 10 Chukchi Sea; 12) East Siberian Sea; 13)
811 Kara Sea; 14) Barents Sea; 15) Fram Strait.

812

813 **Figure 2**. 2D histograms of potential temperature (top panel) and) and DOM fluorescence
814 (bottom panel) against practical salinity for all observations included in the study (0-800m). Note
815 data with temperatures warmer than 6ºC are not shown.

816 **Figure 3.** Section plots along the trajectories of ITP 64 (left column), 48 (middle column) and 93
817 (right column) for salinity (top row), potential temperature (middle row) and DOM fluorescence
818 (bottom row). The links to the map indicate where specific profiles along the trajectory originate
819 from. Note the DOM fluorescence scale is varies and there are data from ITP 48 and 93 that are
820 off scale (above the maximum shown).

821 **Figure 4.** Archetypical water column profiles of a) potential temperature, b) practical salinity and
822 c) DOM fluorescence. The lower panels show property-property plots d) potential temperature
823 against practical salinity (freezing temperature as grey dashed line) and e) DOM fluorescence
824 against salinity. Green-PS94; Magenta-ITP60; Black-ITP48; Blue-ITP48; Red-ITP65; Cyan-
825 ITP64; Brown-NAACOS.

826 **Figure 5.** Histograms of properties of the DOM fluorescence maximum in the halocline (S 31-
827 34). The data are colored with respect to three groups, to illustrate different features: blue-
828 salinity 31-33.2 and DOM fluorescence <0.0305 nm^{-1}; red-salinity 31-33.2 and DOM
829 fluorescence >0.0305 nm^{-1}; yellow-salinity>33.2; a) practical salinity; b) potential temperature;
830 c) DOM fluorescence; d) depth of temperature maximum; e) deviation from freezing
831 temperature; and f) distribution of longitudinal position between groups.

832 **Figure 6.** Histograms of properties of the potential temperature maximum. The data are colored
833 to illustrate different features: blue-salinity >33 and depth between 200 and 370 m; red-
834 salinity<33; yellow-salinity>33; a) practical salinity; b) potential temperature; c) DOM
835 fluorescence; d) depth of temperature maximum; e) deviation from freezing temperature; and f)
836 distribution of longitudinal position between groups.

837 **Figure 7.** Histograms of properties of the potential temperature minimum. The data are colored
838 to illustrate different features: blue - deviation from freezing temperature > 0.2ºC; red - deviation
839 from freezing temperature < 0.2ºC and 31<S<32; yellow - deviation from freezing temperature <
840 0.2ºC and 29.5<S<31; purple - deviation from freezing temperature < 0.2ºC and salinity <29; a)
841 practical salinity; b) potential temperature; c) DOM fluorescence; d) depth of temperature
842 maximum; e) deviation from freezing temperature; and f) distribution of longitudinal position
843 between groups.

844 **Figure 8.** Mean endmembers characteristics from the analysis of temperature maximum (red),
845 temperature minimum (blue) and DOM fluorescence (black) maximum properties plotted
846 together will all data (grey). The error bars indicate standard deviation. The top graph is potential
847 temperature against practical salinity and the bottom graph is DOM fluorescence against
848 practical salinity. The horizontal dashed line represent the 0 ºC isotherm and the vertical line the
849 34 isohaline. The diagonal represents a theoretical mixing line between Siberian shelf water
850 (Gonçalves-Araujo et al., 2016) and Atlantic water.

851 **Figure 9.** Schematic indicating the three major DOM fluorescence pathways in the upper
852 halocline (S<34). The dark brown arrow indicates the low saline (S<33) shelf waters of the TPD
853 with high DOM fluorescence (>0.04 nm^{-1}) that is restricted to the surface 100m.. The light brown
854 arrow indicates higher salinity HL waters (33-34) which are formed as an intermediate between
855 TDP and AW. These extend below the TPD and in the Canada Basin form a layer above warmer
856 Atlantic water. The green arrow indicates the Chuckchi shelf waters which which originate from
857 the Pacific inflow and have high DOM fluorescence from shelf sediments. These lie between a
858 dilute PML with low salinity and DOM fluorescence due to sea ice melt, and the HL originating
859 from the Eurasian Basin. The dark blue indicate AW. Indicated are the average properties from
860 the end member analysis.

861

862 **Table 1.** Summary of the available data after quality control of the profile data. Only profiles
863 with complete records of temperature, salinity and CDOM fluorescence were selected.

Platform	Fluorescence Sensor***	Start (ITP deployment region)	End	# Profiles	Source
ITP48	*ECO* FLbb-CD	10/Sep/2011 (Lomonosov Ridge)	29/Oct/2012	1302	(Laney et al., 2014; Toole et al., 2016)
ITP52	*ECO* FLbb-CD	6/Aug/2011 (Beaufort Sea)	14/Nov/2011	363	(Laney et al., 2014; Toole et al., 2016)
ITP60	*ECO* FLbb-CD	15/Sep/2012 (Amundsen Basin)	23/Dec/2012	259	(Laney et al., 2014; Toole et al., 2016)
ITP64	*ECO* FLbb-CD	29/Aug2012 (Beaufort Sea)	25/Aug/2013	1079	(Laney et al., 2014; Toole et al., 2016)
ITP65	*ECO* FLbb-	28/Aug/2012	18/Feb/2013	397	(Toole et al., 2016)

	CD	(Beaufort Sea)			
ITP69	*ECO* FLbb-CD	29/Aug/2013 (Chukchi Plateau)	15/Feb/2014	343	(Toole et al., 2016)
ITP72	*ECO* FLbb-CD	31/Aug/2013 (Amundsen Basin)	16/Dec/2013	216	(Toole et al., 2016)
ITP93	*ECO* FLbb-CD	24/Sep/2015 (Lomonosov Ridge)	8/Aug/2016	944*	(Toole et al., 2016)
PS94	DrHaardt	18/Aug/2015	9/Oct/2015	81**	(Rabe et al., 2016a, 2016b)
NAACOS	WETStar	3/Sep/2012	12/Sep/2012	60	Stedmon in prep

*Profiles after profile 955 are not included due to failure in the conductivity sensor.
** Data from depths greater than 800m (max depth covered by ITPs) are not included in the analysis.
***ECO FLbb-CD and WETStar (WET Labs Inc.): Excitation 370 and emission 460 nm; DrHaardt: Excitation 350 – 460 nm, emission 550 nm.

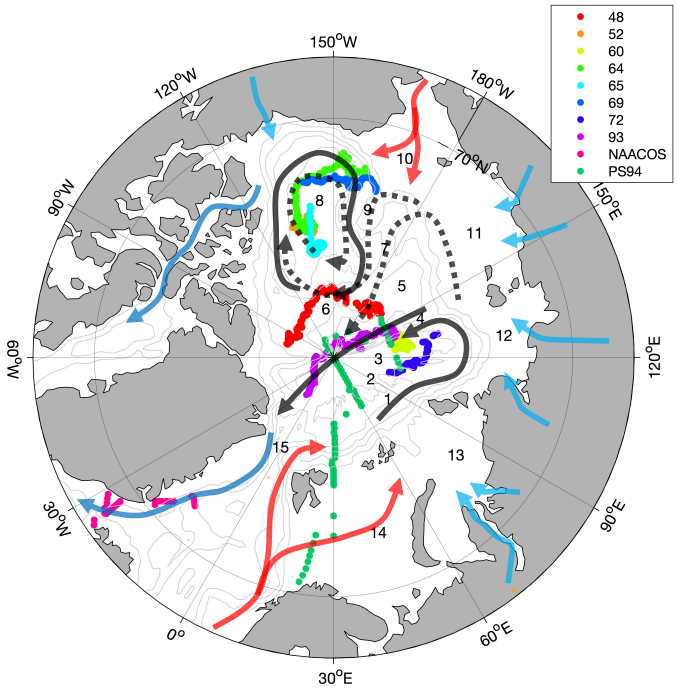

Figure 1: ITP drift pathways, cruise stations and schematic of general circulation pathways. Red arrow indicate inflowing ocean water; Blue arrows polar water exiting Arctic, Light-blue major Arctic rivers. Black indicates two features of the central Arctic, Transpolar drift extending from shelf and passing over the pole, and the Beaufort Gyre. Solid and dotted lines indicate position of these under positive and negative Arctic Oscillation (Morison et al 2012). Legend indicates the ITP and cruise identity. The numbers on the map indicate areas: 1) Nansen Basin; 2) Gakkel Ridge; 3) Amundsen Basin; 4) Lomonosov Ridge; 5) Makarov Basin; 6) Alpha Ridge; 7) Mendelev Ridge; 8 Beaufort Sea; 9 Chukchi Plateau; 10 Chukchi Sea; 12) East Siberian Sea; 13) Kara Sea; 14) Barents Sea; 15) Fram Strait.

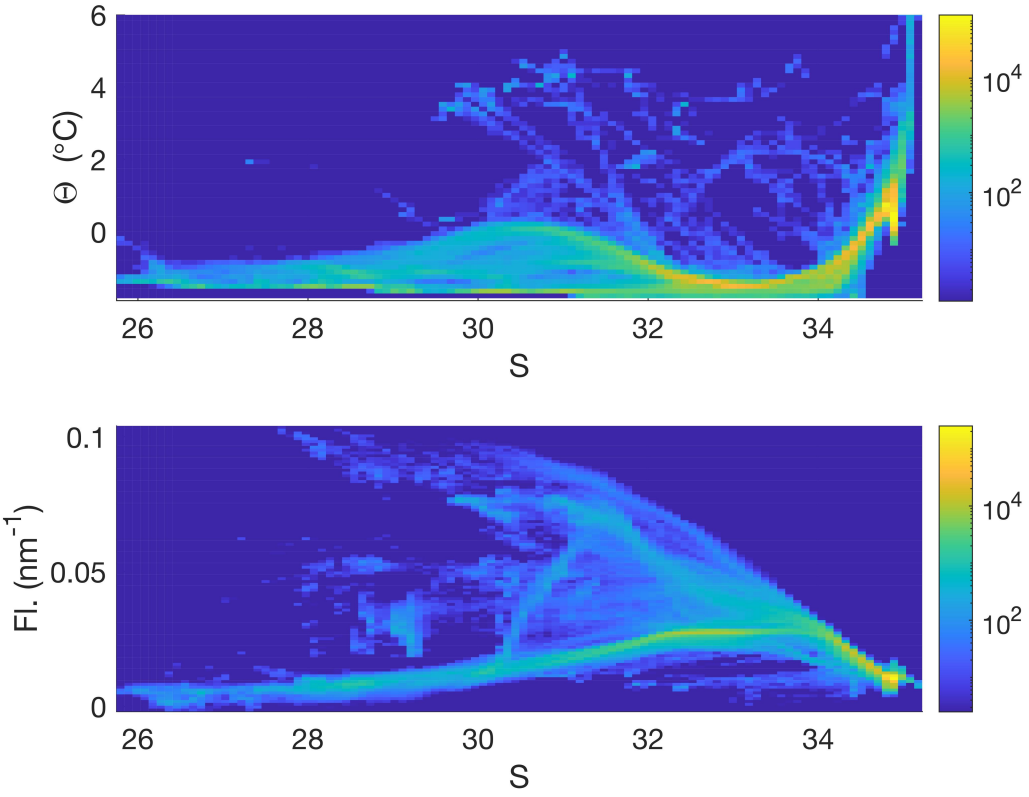

Figure 2. 2D histograms of potential temperature (top panel) and) and DOM fluorescence (bottom panel) against practical salinity for all observations included in the study (0-800m). Note data with temperatures warmer than 6ºC are not shown.

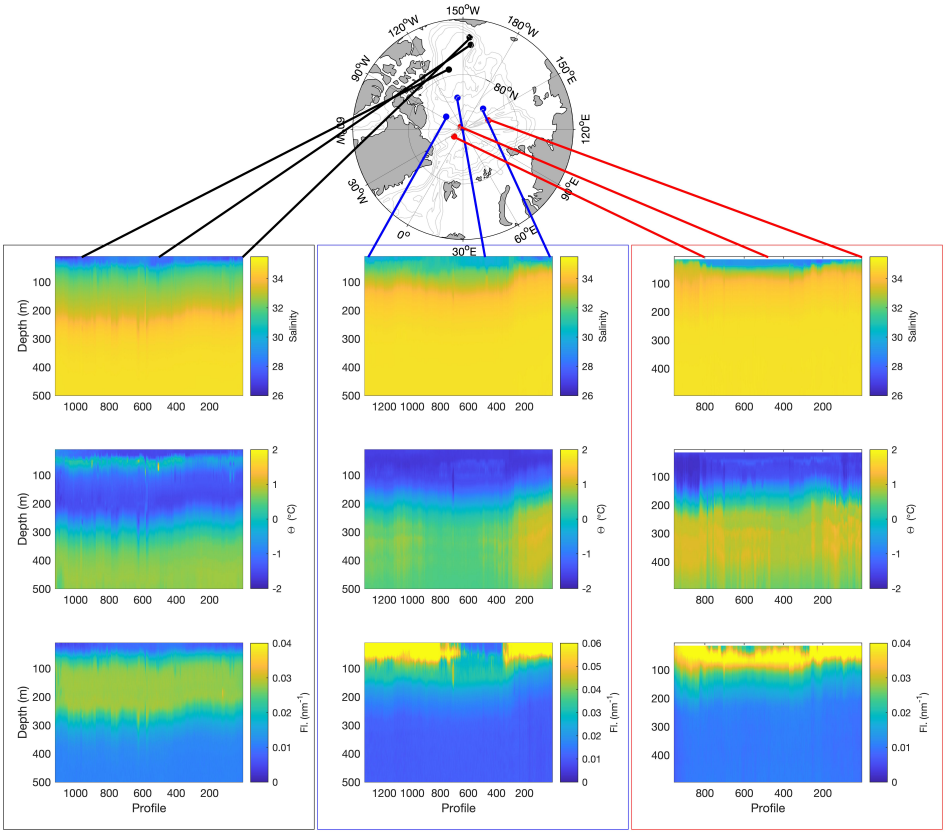

Figure 3. Section plots along the trajectories of ITP 64 (left column), 48 (middle column) and 93 (right column) for salinity (top row), potential temperature (middle row) and DOM fluorescence (bottom row). The links to the map indicate where specific profiles along the trajectory originate from. Note the DOM fluorescence scale is varies and there are data from ITP 48 and 93 that are off scale (above the maximum shown).

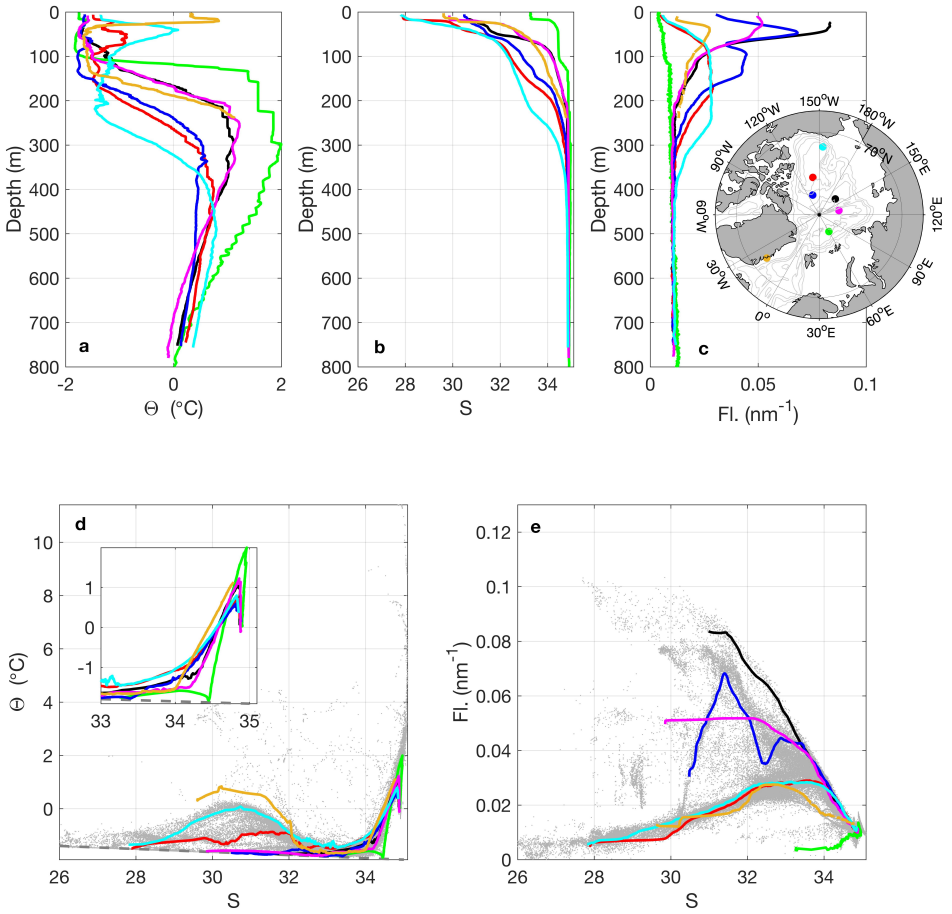

Figure 4. Archetypical water column profiles of a) potential temperature, b) practical salinity and c) DOM fluorescence. The lower panels show property-property plots d) potential temperature against practical salinity (freezing temperature as grey dashed line) and e) DOM fluorescence against salinity. Green-PS94; Magenta-ITP60; Black-ITP48; Blue-ITP48; Red-ITP65; Cyan-ITP64; Brown-NAACOS.

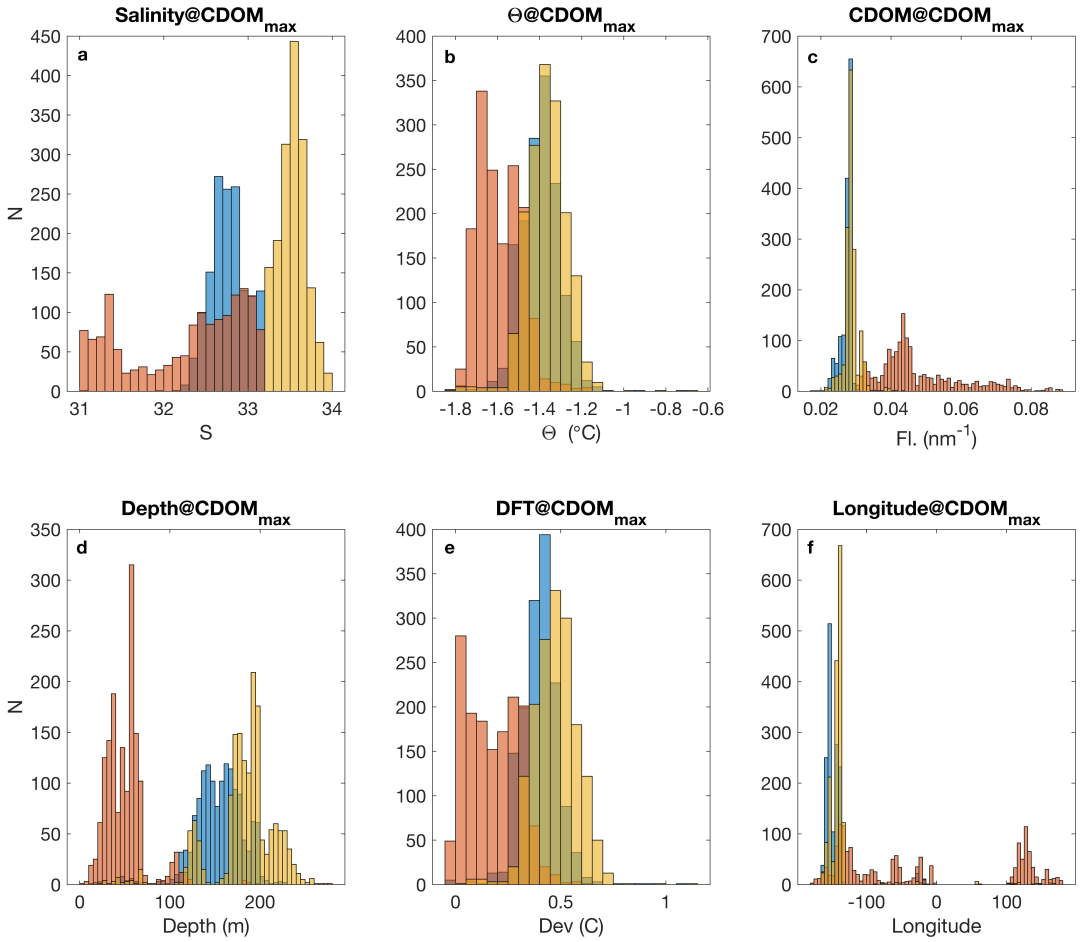

Figure 5: Histograms of properties of the DOM fluorescence maximum in the halocline (S 31-34). The data are colored with respect to three groups, to illustrate different features: blue-salinity 31-33.2 and DOM fluorescence <0.0305 nm^{-1}; red-salinity 31-33.2 and DOM fluorescence >0.0305 nm^{-1}; yellow-salinity>33.2; a) practical salinity; b) potential temperature; c) DOM fluorescence; d) depth of temperature maximum; e) deviation from freezing temperature; and f) distribution of longitudinal position between groups.

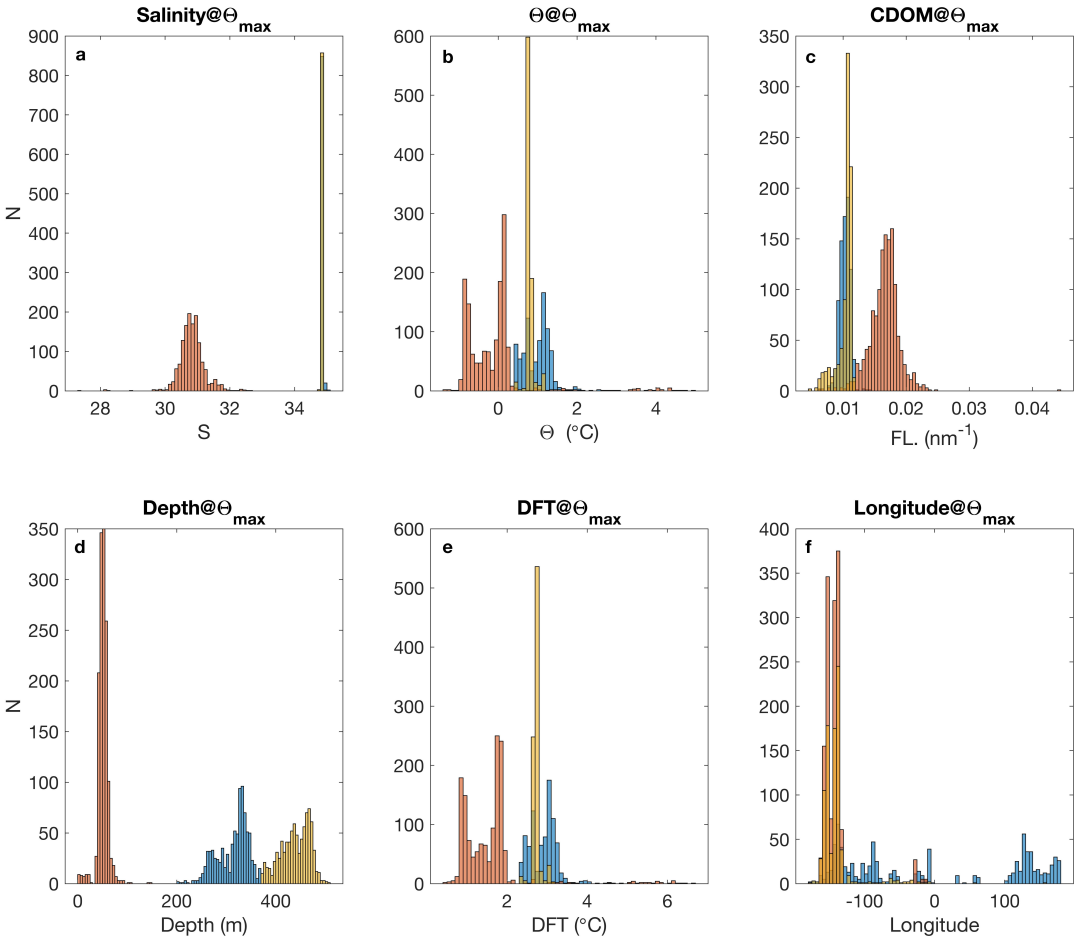

Figure 6: Histograms of properties of the potential temperature maximum. The data are colored to illustrate different features: blue-salinity >33 and depth between 200 and 370 m; red-salinity<33; yellow-salinity>33; a) practical salinity; b) potential temperature; c) DOM fluorescence; d) depth of temperature maximum; e) deviation from freezing temperature; and f) distribution of longitudinal position between groups.

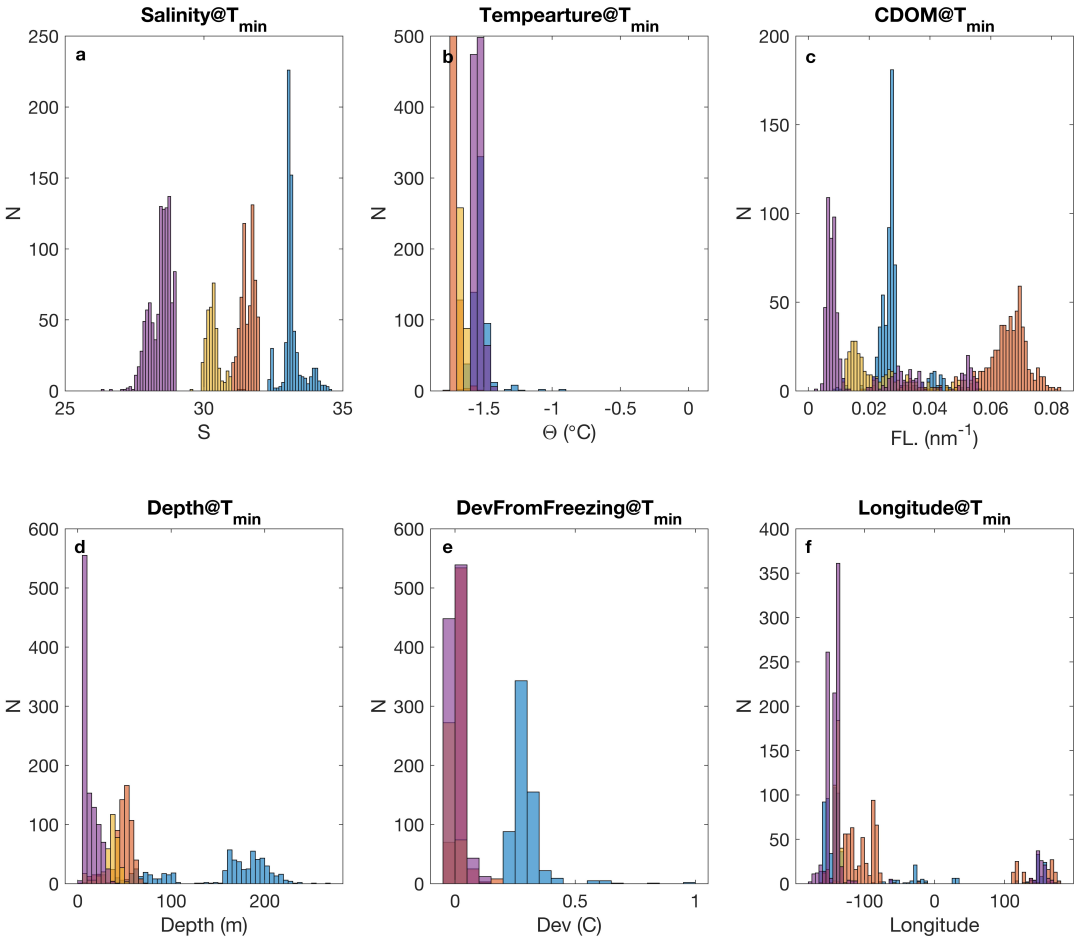

Figure 7: Histograms of properties of the potential temperature minimum. The data are colored to illustrate different features: blue - deviation from freezing temperature > 0.2ºC; red - deviation from freezing temperature < 0.2ºC and 31<S<32; yellow - deviation from freezing temperature < 0.2ºC and 29.5<S<31; purple - deviation from freezing temperature < 0.2ºC and salinity <29; a) practical salinity; b) potential temperature; c) DOM fluorescence; d) depth of temperature maximum; e) deviation from freezing temperature; and f) distribution of longitudinal position between groups.

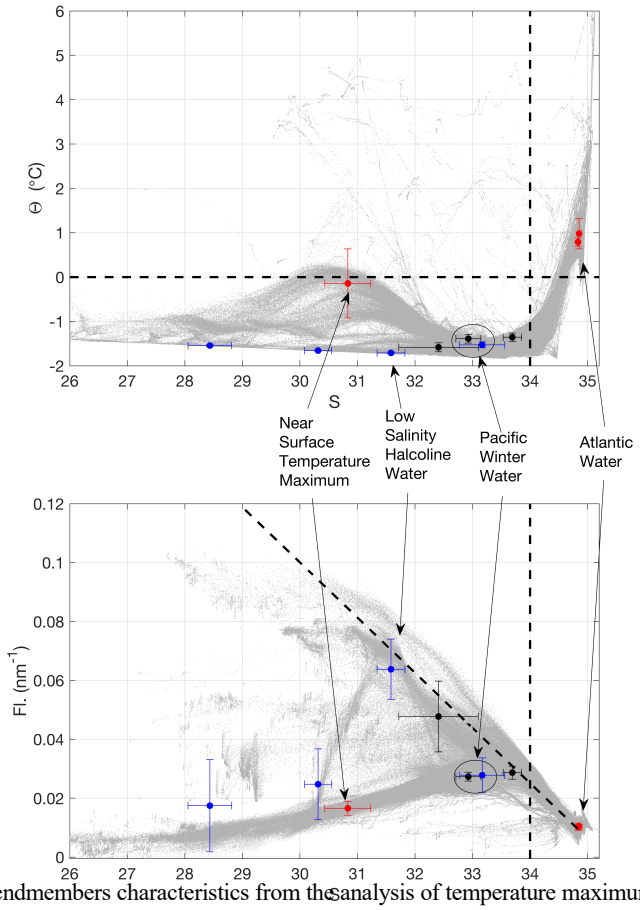

Figure 8: Mean endmembers characteristics from the analysis of temperature maximum (red), temperature minimum (blue) and DOM fluorescence (black) maximum properties plotted together will all data (grey). The error bars indicate standard deviation. The top graph is potential temperature against practical salinity and the bottom graph is DOM fluorescence against practical salinity. The horizontal dashed line represent the 0 degree isotherm and the vertical line the 34 isohaline. The diagonal represents a theoretical mixing line between Siberian shelf water (Gonçalves-Araujo et al., 2016) and Atlantic water.

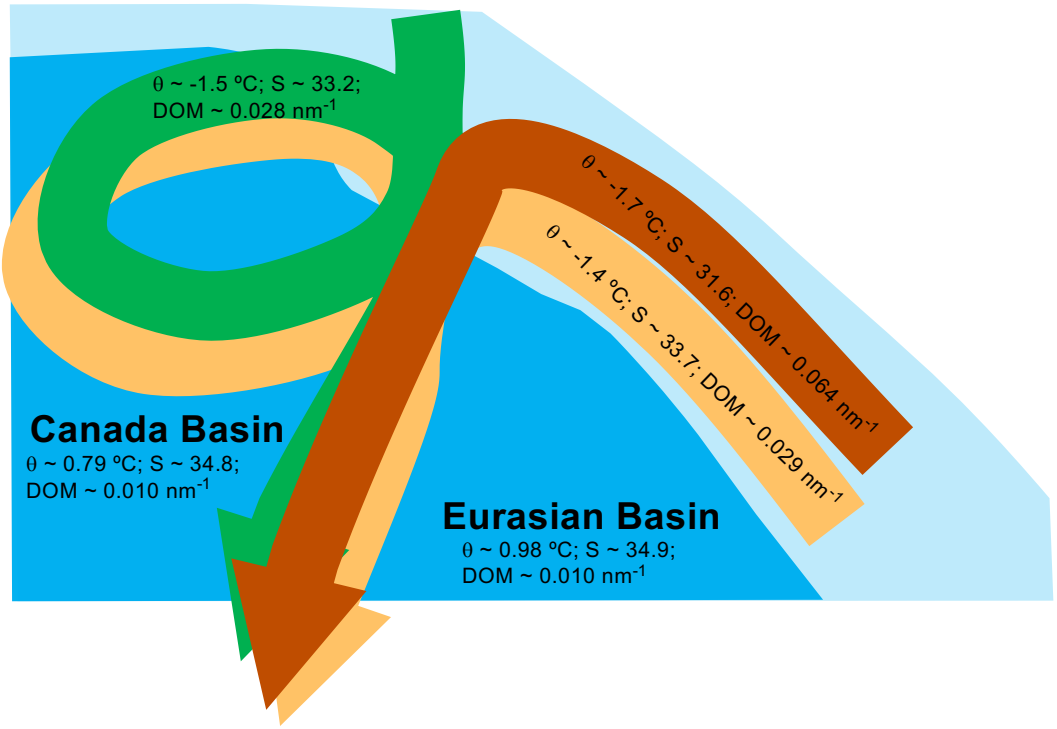

Figure 9: Schematic indicating the three major DOM fluorescence pathways in the upper halocline (S<34). The dark brown arrow indicates the low saline (S<33) shelf waters of the TPD with high DOM fluorescence (>0.04 nm^{-1}) that is restricted to the surface 100m.. The light brown arrow indicates higher salinity HL waters (33-34) which are formed as an intermediate between TDP and AW. These extend below the TPD and in the Canada Basin form a layer above warmer Atlantic water. The green arrow indicates the Chuckchi shelf waters which which originate from the Pacific inflow and have high DOM fluorescence from shelf sediments. These lie between a dilute PML with low salinity and DOM fluorescence due to sea ice melt, and the HL originating from the Eurasian Basin. The dark blue indicate AW. Indicated are the average properties from the end member analysis.

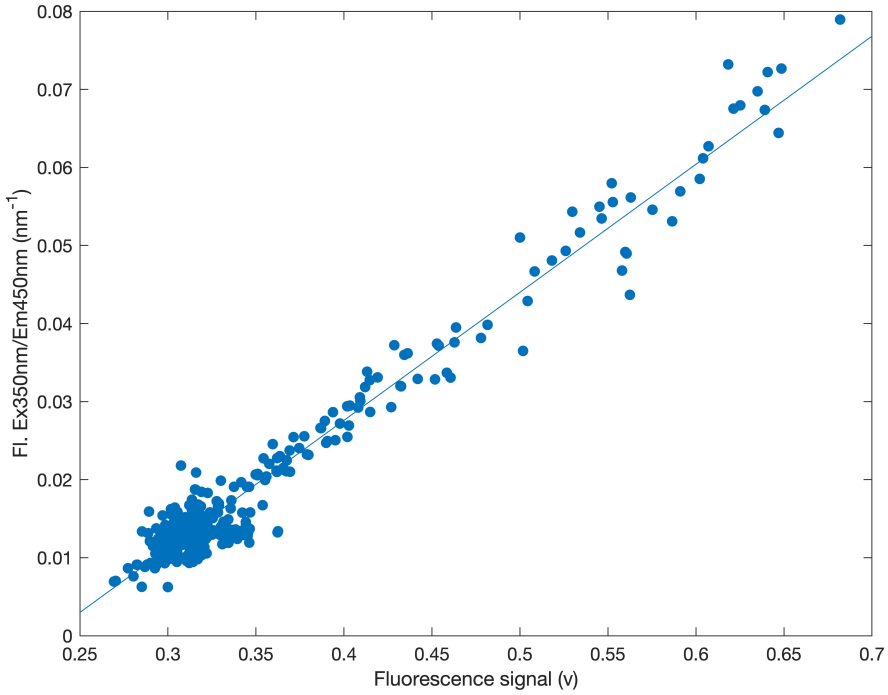

Figure S1. Calibration of the CTD mounted fluorometer on PS94 to water samples taken and measured onboard. Fl. = V * 0.1641 – 0.0380; $R^2 = 0.96$.

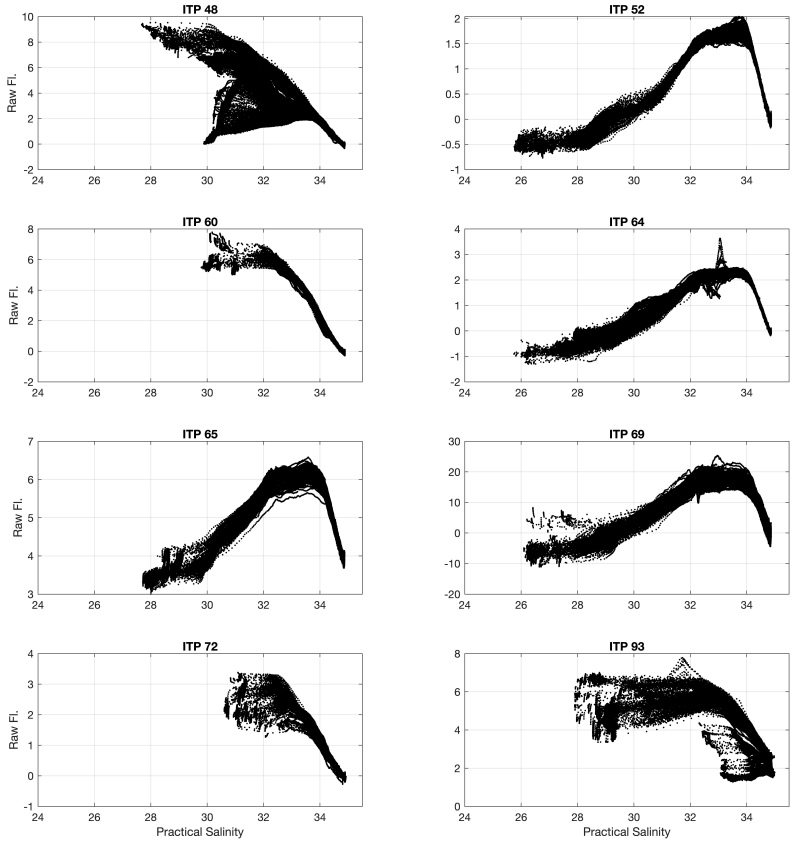

Figure S2. Raw fluorescence signal from the ITPs.

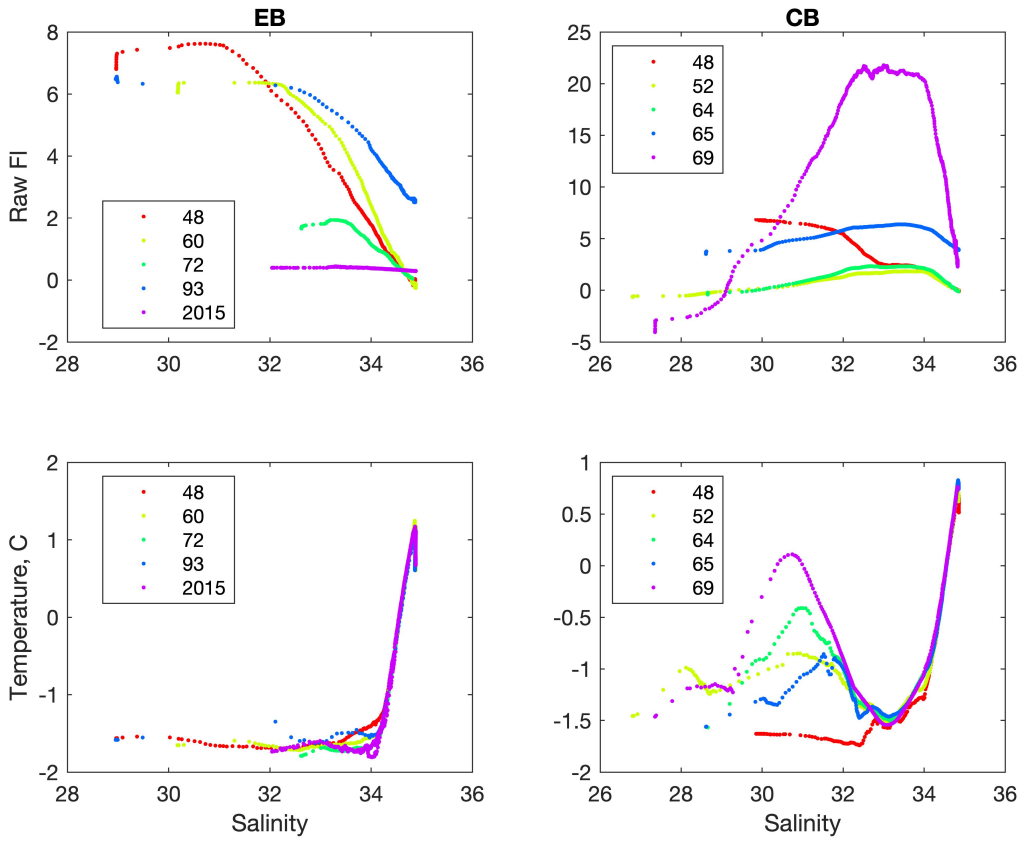

Figure S3. Data from selected profiles for Eurasian (EB) and Canada Basins (CB), where waters with common T-S were sampled and could be used to intercalibrate DOM fluorescence signal.

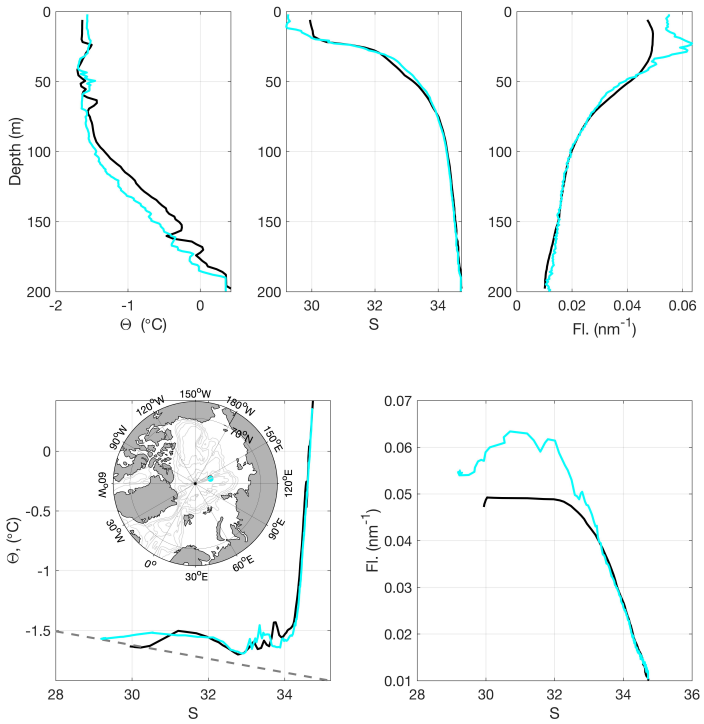

Figure S4. Comparison of PS94 (blue) with ITP93 calibrated using the T-S space approach for a station where ITP93 was deployed and a ship CTD cast was also performed.

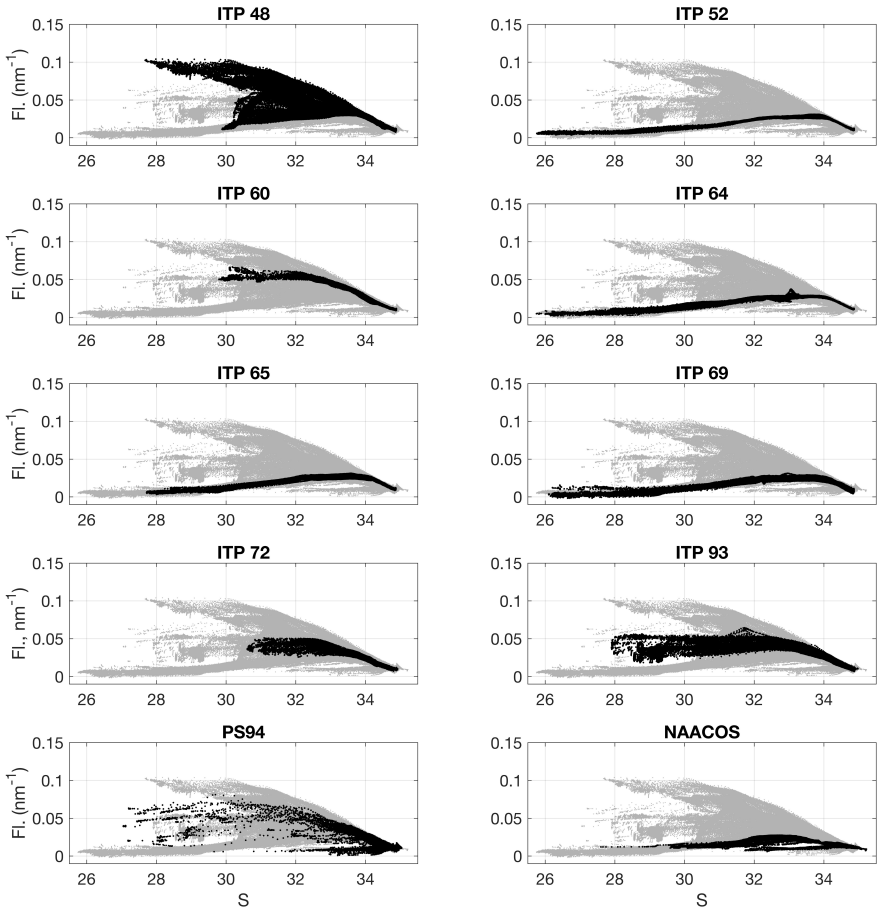

Figure S5: Calibrated organic matter fluorescence against practical salinity. Black data are for each specific ITP or cruise. Grey data points in the background are all data combined.